GEOLOGICA CARPATHICA, 2024, 75, 4, 243–269 https://doi.org/10.31577/GeolCarp.2024.13

Implication of Cenozoic tectono-sedimentary evolution for the geoenergy potential in the NW Transcarpathian Basin

VIKTÓRIA SUBOVÁ[1,✉], SAMUEL RYBÁR[1,2], NATÁLIA HUDÁČKOVÁ[1], MICHAL JAMRICH[1], FRED JOURDAN[3,4], CELIA MAYERS[3] and ĽUBOMÍR SLIVA[5]

[1]Department of Geology and Paleontology, Faculty of Natural Sciences, Comenius University Bratislava, Mlynská dolina, Ilkovičova 6, 842 15 Bratislava, Slovakia
[2]Technical University of Ostrava, Faculty of Mining and Geology, Department of Geodesy and Mine Surveying, 17. listopadu 2172/15, 708 00 Ostrava Poruba, Czech Republic
[3]School of Earth and Planetary Sciences, SSTC and TIGeR, Curtin University, Perth, Western Australia 6845, Australia
[4]Western Australian Argon Isotope Facility and John de Laeter Centre, Curtin University, Perth, Western Australia 6845, Australia
[5]NAFTA a.s., Plavecký Štvrtok 900, 900 68 Plavecký Štvrtok, Slovakia

(Manuscript received April 29, 2024; accepted in revised form August 27, 2024; Associate Editor: Michal Šujan)

Abstract: The extensive Pannonian Basin System comprises several hydrocarbon-bearing sub-basins, including the moderately explored Transcarpathian Basin located in its NW part. Tectono-sedimentary and volcanic events have influenced the sub-basin's infill and geoenergy potential. Through a comprehensive analysis of petrophysical, organic geochemical, sedimentological, and biostratigraphic data, we aim to uncover the characteristics of petroleum and geothermal plays in the challenging-to-sample Prešov depocenter (NW corner of the Transcarpathian Basin) and its surrounding areas. The results highlight two significant tectono-sedimentary events: first, the opening and subsequent disintegration of the compressional foreland Central Carpathian Paleogene Basin, and its Lower Miocene continuation, which facilitated the deposition of source rocks. Second, the initial phase of rifting in the transtensional Prešov sub-basin, part of a broader back-arc system, created accommodation space for Karpatian to Badenian (Burdigalian to Serravallian) facies. This process led to the formation of fault system that deformed whole sedimentary infill, including the pre-Cenozoic basement carbonates, which resulted in the creation of structural traps and pathways for horizontal and vertical migration. This research reaffirms the geoenergy potential of Paleogene sedimentary records in Central Europe as viable source rocks for hydrocarbons. Contrary to established knowledge, organic lean kerogen type III appears to not only produce methane gas but also wet gas. A promising hydrocarbon trap has been identified in the Triassic to basal Paleogene carbonate breccia reservoirs, though it includes a risk of CO_2 and N_2 contamination. Notably, this risk diminishes in the uppermost sections of the carbonate traps, where the highest concentrations of methane and wet gas are found, likely due to the gravitational separation of gases by molecular weight. Additionally, these carbonate breccias show moderate geothermal potential.

Keywords: Transcarpathian Basin, tectono-sedimentary evolution, geoenergy potential, reservoir and source rocks, geothermal

Introduction

The vast Neogene Pannonian Basin System (PBS; Fig. 1a) in Central Europe is bordered by the Carpathian Mountains, Alps, and Dinarides (Royden & Horváth 1988; Tari et al. 1993; Horváth 1995; Horváth et al. 2006; Schmid et al. 2008; Balázs et al. 2016; Fodor et al. 2021). The origin of this area is influenced by complex processes, starting with the convergence of the African and Eurasian plates during the late Mesozoic, leading to creation of the Alpine orogen (Csontos & Vörös 2004; Horváth et al. 2006). The ongoing convergence resulted in lateral extrusion of the Carpathians from the Alps towards to the East during the Cenozoic (Ratschbacher et al. 1991a, b). This process resulted in formation of the Neogene Pannonian back-arc Basin System. The system experienced extensive subsidence, sedimentation (Horváth 1995; Horváth et al. 2006; Balázs et al. 2016; Cloetingh et al. 2021; Fodor et al. 2021; Tari et al. 2021) and volcanic activity due to the attenuated mantle (Pécskay et al. 2006; Harangi & Lenkey 2007; Lexa et al. 2010; Lukács et al. 2018, 2024). These processes, occurring from the Miocene to Quaternary, facilitated the formation of deep basins or sub-basins characterized by low-angle detachment faults and metamorphic core complexes (Royden & Horváth 1988; Soták et al. 1999; Fodor et al. 2021; Babinszki et al. 2023). An excellent example of such is the Transcarpathian Basin (TB; Fig. 1a), located in the north-eastern segment of the PBS, extending from Slovakia through Ukraine, Romania, and partly Hungary (Horváth 1995). The Slovak part of Transcarpathian Basin (STB), also known as East Slovakian Basin, represents an important depocenter divided by the Neogene volcanic Slanské vrchy Mountains into two sub-basins (Fig. 1b): (1) Trebišov sub-basin, with

✉ corresponding author: Viktória Subová
viki.subova96@gmail.com

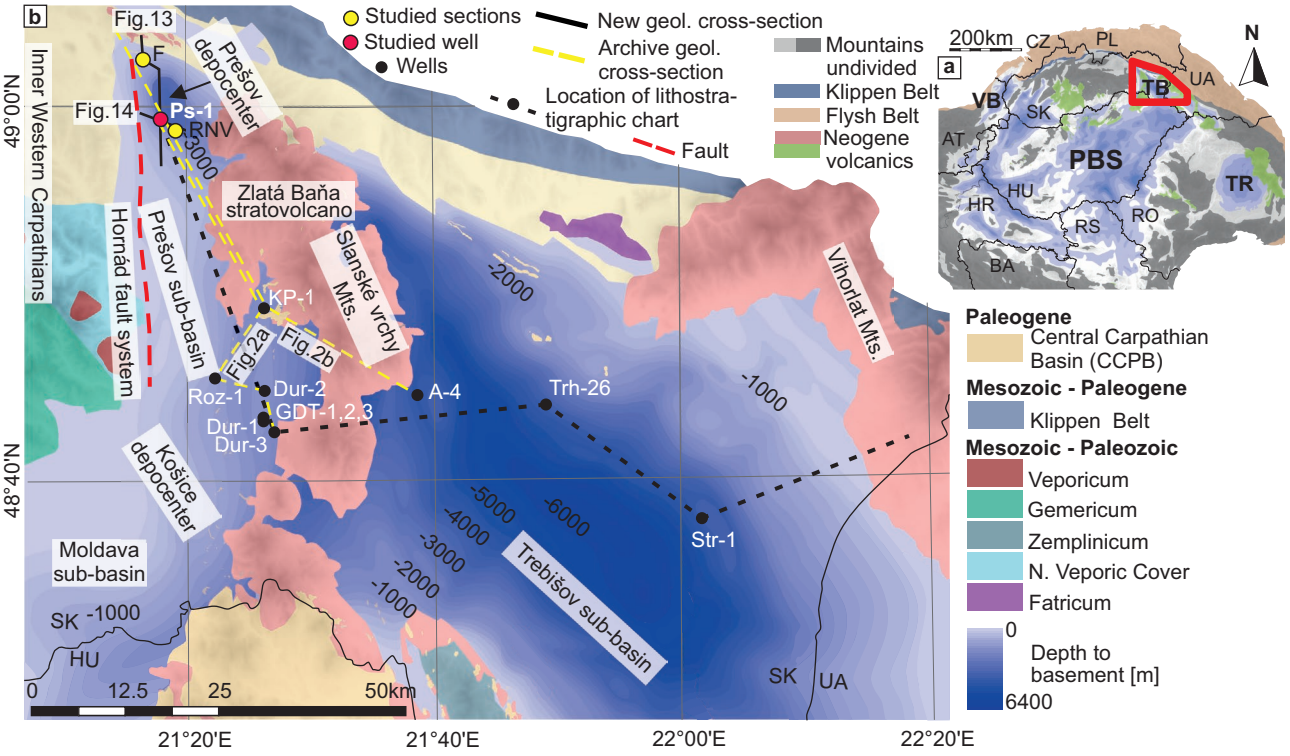

Fig. 1. a — Location of the Transcarpathian Basin (TB) within the Pannonian Basin System (PBS). Abbreviations: VB=Vienna Basin; TR=Transylvanian Basin; SK=Slovakia; PL=Poland; CZ=Czechia; UA=Ukraine; AT=Austria; HU=Hungary; RO=Romania; RS=Serbia; HR=Croatia; BA=Bosnia and Herzegovina. **b** — Detailed map of the Slovak part of Transcarpathian Basin with highlighted sections: F=Fintice; RNV=Ruská Nová Ves, and deep wells (Table 1). Modified after Rudinec (1960, 1965, 1983); Čverčko (1969, 1970, 1975); Fusán et al. (1987); Vranovská (2001); Vranovská et al. (2012); Hók et al. (2014) and Horváth et al. (2015).

a total sediment thickness of 6–7 km (Řeřicha & Rudinec 1979; Fusán et al. 1987), and (2) Prešov sub-basin with a sediment thickness of 3 km or more (Fusán et al. 1987).

The TB is one of the Neogene sedimentary basins of Slovakia, which yields hydrocarbons (Rudinec 1976). Gas production predominates and hydrocarbon generation zones were only found in sediments older than upper Sarmatian (Franců et al. 1990; Milička et al. 2011). Source rocks can be associated with Paleogene and/or Badenian–Sarmatian shales (Franců et al. 1989). Reservoir rocks in the basin are mostly found in Miocene sandstones deposited in a deltaic environment (Janočko 2004), and rarely in Triassic carbonates (Čverčko 1969, 1970; Rudinec 1983). Hundreds of deep wells have been drilled for hydrocarbon exploration in the Trebišov sub-basin (e.g., Stretava-1, Trhovište-26; Fig. 1b; Table 1; Rudinec 1976). Nonetheless, only one deep well exists in the unexplored Prešov depocenter (Prešov-1 well; Ps-1; Fig. 2a, b; Table 1). The migration from the source rock to the reservoir was never elaborated. Due to the low volume of methane (CH_4) and high content of carbon dioxide (CO_2) together with nitrogen (N_2), further drilling in the past was not recommended due to economic reasons, so the Prešov depocenter was abandoned (Čverčko 1975). Nevertheless, at the current stage of petroleum industry, this depocenter can become attractive.

Table 1: GPS location of the studied and discussed deep wells within the TB basin.

Abbreviation	Name	Lattitude	Longitude
A-4	Albínov-4	48°44'32.5474"N	21°38'45.5075"E
Dur-2	Ďurkov-2	48°44'48.288"N	21°26'19.304"E
Dur-3	Ďurkov-3	48°42'39.934"N	21°27'0.413"E
GDT-1	Ďurkov-1	48°43'20.567"N	21°26'16.954"E
GDT-2	Ďurkov-2	48°43'20.475"N	21°26'17.156"E
GDT-3	Ďurkov-3	48°43'20.567"N	21°26'16.954"E
KP-1	Kecerovské Pekľany-1	48°49'14.5882"N	21°26'14.6145"E
Ps-1	Prešov-1	48°59'25.6753"N	21°17'53.8425"E
Roz-1	Rozhanovce-1	48°45'27.527"N	21°22'13.972"E
Str-1	Stretava-1	48°37'49.5616"N	22°01'28.8827"E
Trh-26	Trhovište-26	48°44'0.5969"N	21°48'44.5291"E

The investigated area also seems to include suitable geological conditions for geothermal prospects that can be applied in the renewable energy sector. Geothermal waters were found in deep wells originally intended for hydrocarbon exploration, e.g., Ďurkov-1, Ďurkov-3, Kecerovské Pekľany-1 and Prešov-1 wells (Fig. 1b, Table 1; Rudinec 1989). The geothermal activity of the Prešov sub-basin is also highlighted by the natural spring of geothermal waters in Košice (Košice depocenter; Fig. 1b, 2; Franko et al. 1995). Due to the thinned crust

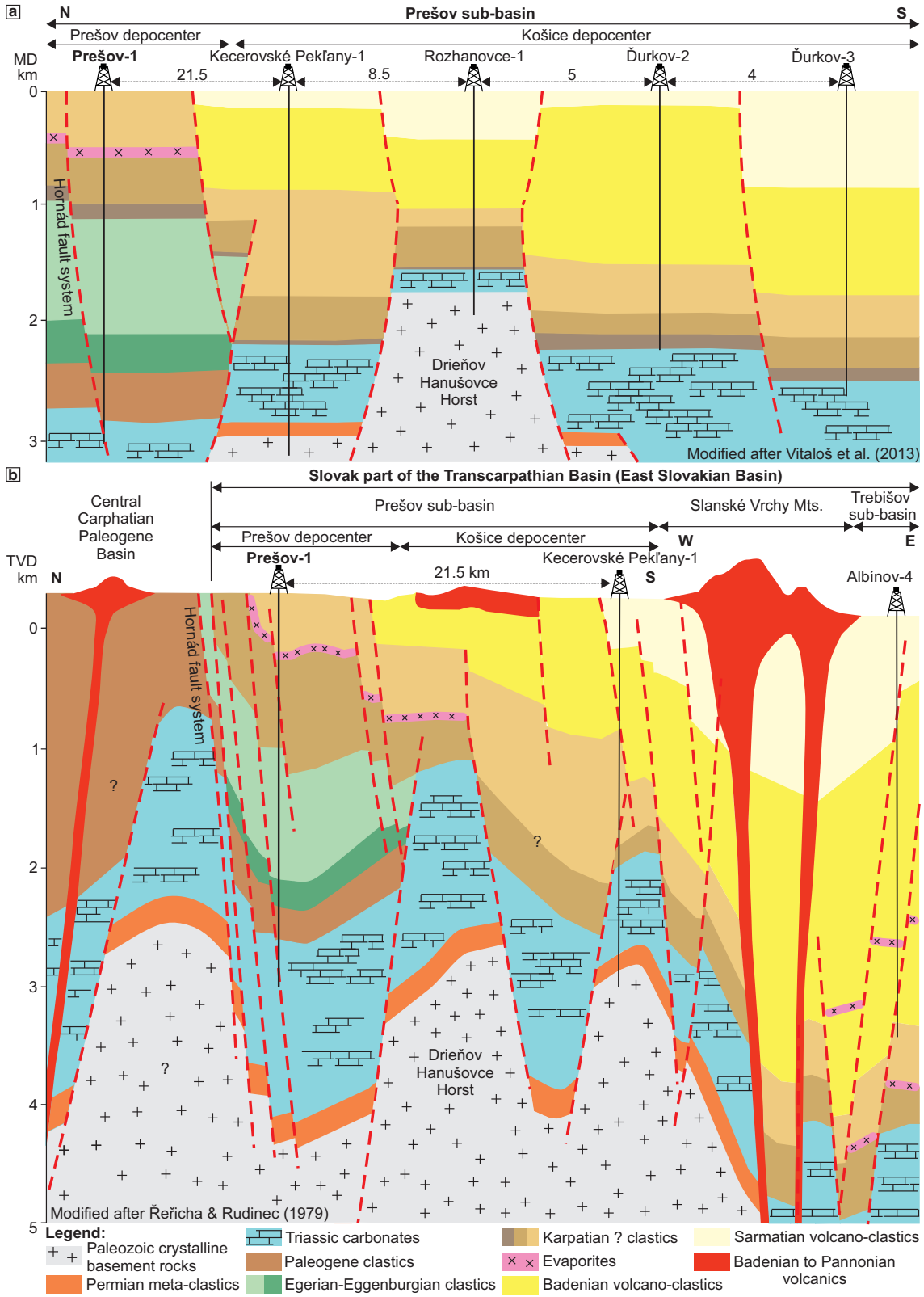

Fig. 2. a — Cross-section through the Prešov sub-basin with deep wells drilled in the Prešov and Košice depocenters. **b** — Geological cross-section highlighting volcanic bodies within the Slovak part of Transcarpathian Basin. For profile and well locations see Fig. 1b and Table 1. Modified after Řeřicha & Rudinec (1979) and Vitaloš et al. (2013).

under the basin and the intensive volcanic activity during the Badenian to Pannonian (Kaličiak 1980), the heat flow is very high (110 mW/m^2; Franko et al. 1995), and the geothermal gradient reaches 53 °C/km (Král et al. 1985; Vass et al. 2005). Source of geothermal waters are primarily connected to Triassic dolomites with a thickness of 300 m to more than 1000 m (Franko et al. 1995; Jacko et al. 2021). In a depth between 500–4000 m, the average temperature of the geothermal waters in the reservoirs ranges from 29 to 178 °C (Remšík 1993). Deep well aquifers are of different types (26,800–33,400 mg/l Total Dissolved Solids=TDS; in the Ďurkov-1 and Kecerovské Pekľany-1 wells) characterized by marinogenic mineralization, which can be degraded by rainwater infiltration (Franko et al. 1995). A good example of the use of geothermal energy is the Ďurkov field, where 3 wells were recently drilled, namely GTD-1, GTD-2, and GTD-3 (Fig. 1b, 3, Table 1; Vranovská 2001; Jacko et al. 2021). Although, the Košice depocenter is assumed to be an area with the highest potential for efficient utilization of geothermal energy (Jacko et al. 2021), the Prešov depocenter with the same potential is less explored.

Regardless of the geofluid type (hydrocarbons, geothermal), petrophysical parameters (porosity and permeability) are always necessary for a detailed understanding of the reservoir rocks. Effective porosity excludes isolated pores, which do not contribute to permeability. Ineffective porosity includes all pore spaces within the rock (connected and isolated; Dandekar 2013). The most common porosity analyses are represented by (1) image analysis (e.g., total optical porosity, TOP) offering the advantage of determining the distribution of pore sizes and the morphology of the pores. Yet, this method does not differentiate between effective and ineffective porosity. Moreover, its reliability is somewhat diminished compared to Hg porosimetry. (2) conversely, mercury porosimetry enables the determination of effective porosity with high precision (Andreola et al. 2000). Consequently, the correlation between TOP and Hg porosimetry is crucial.

The main aim of this work is to evaluate the Prešov depocenter with its key sections supplemented by a single existed deep well, to understand the tectono-sedimentary development. Subsequently, this work intends to reveal the hydrocarbon system and geothermal possibilities of this area.

Geological setting

The Slovak part of Transcarpathian Basin (STB) is located in the NE part of the PBS and represents an important sub-basin utilized for geoenergy exploration and extraction. The pre-Cenozoic basement of the Prešov sub-basin includes diverse rock formations. The central part of the sub-basin is mainly composed of Mesozoic and late Paleozoic cover (Veporicum, Tatricum) and nappe units (Fatricum) of the Western Carpathians (Fig. 1a, b, 4; Hók et al. 2014). The southern part includes metamorphic schists (Veporicum) and Paleozoic rocks (Gemericum; Fusán et al. 1987; Hók et al. 2014).

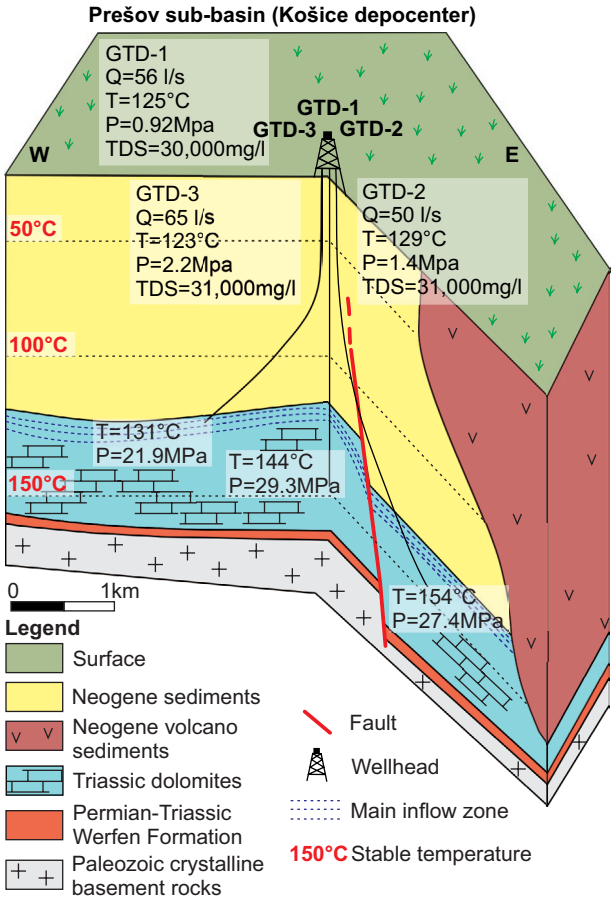

Fig. 3. Schematic geological profile of deep wells GTD-1, 2, 3 in the hydrogeothermal structure of Ďurkov. Modified after Vranovská (2001).

The transpressional strike-slip zone of the Pieniny Klippen Belt (Fig. 1), situated between the external and internal Western Carpathians, separates the Paleogene deposits into the northern Magura Unit and the southern Central Carpathian Paleogene Basin (Rudinec 1980; Gross et al. 1984; Soták et al. 2001; Soták 2010; Starek et al. 2019). The Paleogene rocks of the Hungarian Paleogene Basin are located at the southwestern margin of the area (Báldi & Báldi-Beke 1985, Báldi-Beke & Báldi 1991; Tari et al. 1993; Vass 2002; Hók et al. 2014; Körmös 2021). The Central Carpathian Paleogene Basin (CCPB; Fig. 2) consists of post-kinematic sequences atop folded basement units shaped by pre-Senonian thrusting. It is interpreted either as a remnant forearc basin (Tari et al. 1993) or a foreland basin of the Central Western Carpathians (Soták et al. 2001; Kázmér et al. 2003; Soták 2010; Plašienka & Soták 2015; Starek et al. 2019). Basin formation commenced during the Eocene (Lutetian) due to regional tectonic subsidence (Gross et al. 1984; Köhler & Salaj 1997; Vass 2002) and continued until the latest Oligocene to earliest Miocene (Soták et al. 1996; Subová et al. 2024). The CCPB's Paleogene lithostratigraphic formations, part of the Subtatric Group, are preserved in several structural sub-basins (Gross et al. 1984; Soták et al. 2001). The sedimentary sequence starts with basal

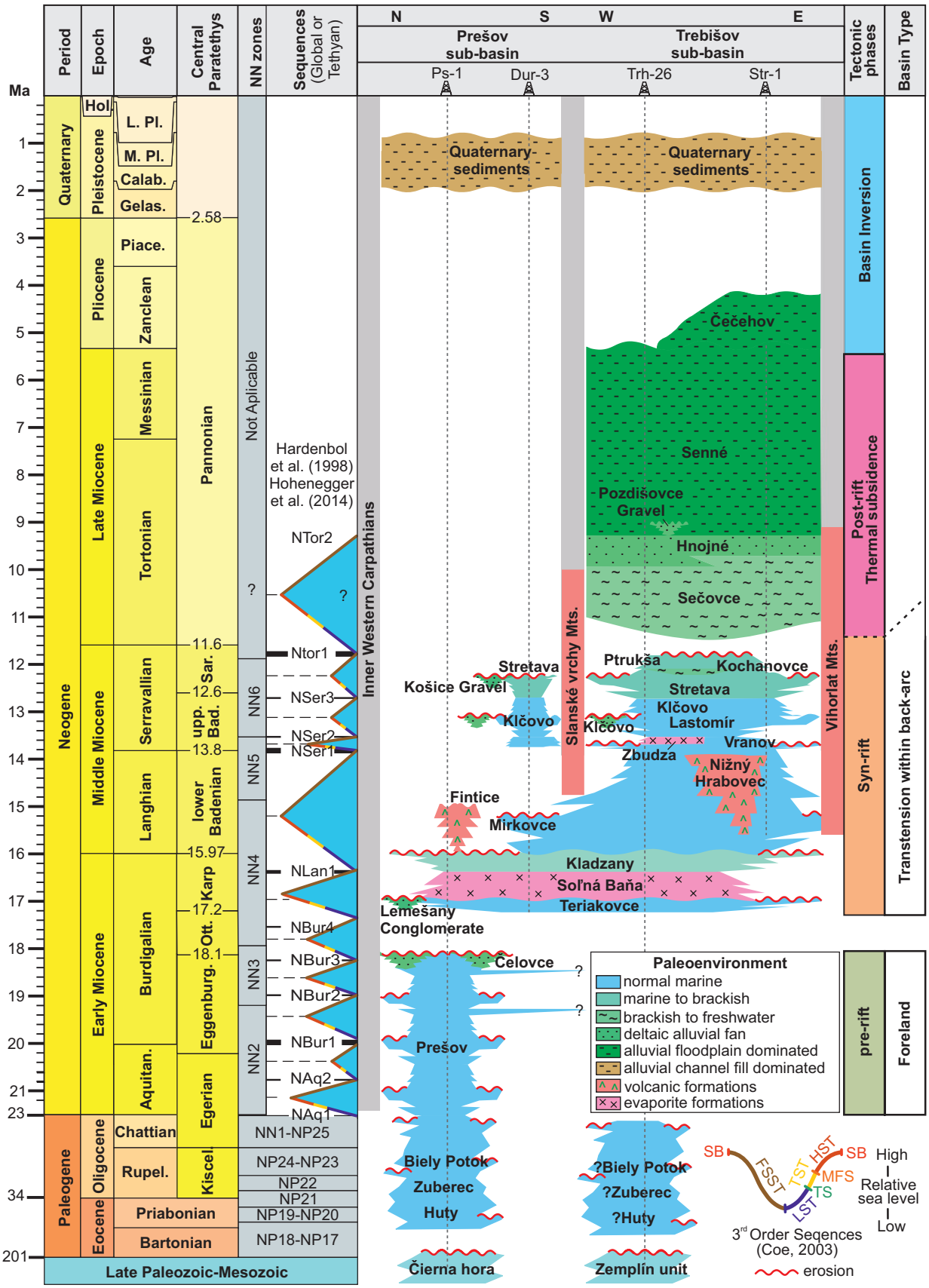

Fig. 4. Lithostratigraphic table of the Slovak part of Transcarpathian Basin. Modified after Kováč (2000); Vass (2002); Vass et al. (2005); Kováč et al. (2007).

transgressive facies comprising breccias, conglomerates, and limestones, transitioning to a carbonate platform (Borové Fm.; Lutetian–Priabonian; thickness: ~220 m; Soták et al. 2001). This is followed by shaly flysch lithofacies (Huty Fm.; Priabonian; ~1200 m), including the notable "menilite" facies. Subsequent significant subsidence allowed facies progradation and subaqueous density flow sedimentation (Soták 1998). The sequence transitions to sandy flysch facies (Zuberec Fm.; Priabonian–Rupelian; ~1000 m). The Paleogene sedimentary sequence concludes with massive sandstone beds interspersed with rare mudstones deposited in a deep sea supra-fan (Biely Potok Fm.; Priabonian–Rupelian; up to 3000 m; Gross et al. 1984). Coarse-grained fan sediment interbeds (Pucov Member; ~250 m) are present across all Paleogene formations (Soták 1998, 2001). During the late Oligocene, reduced tectonic subsidence and relative sea level fall exposed the deep-sea turbidite fan deposits, leading to extensive erosion of the CCPB's uppermost parts during the Neogene and Quaternary (Soták 1998, 2001). Sedimentation might have continued up to the Eggenburgian (Aquitanian–Burdigalian; Fig. 2; Subová et al. 2024). During this time, two formations were deposited: (a) sandy mudstones interbedded with fine-grained sandstones and altered rhyolite tuff in shelf setting (Prešov Fm.; ~1000 m; Biela 1978; Vass 2002), and (b) an alternation of coastal mudstones, sandstones, and conglomerates influenced by deltaic progradation (Čelovce Fm.; ~400 m; Vass 2002). A regional erosional surface atop this sequence marks the transition to the Pannonian Basin System evolution (Kráľ et al. 1990; Vass 2002; Vass et al. 2005).

The sedimentary fill of the Slovak part of the Transcarpathian Basin sensus stricto began forming in the Karpatian (upper Burdigalian; Fig. 2) with a transition from a compressional to a transtensional regime (Kráľ et al. 1990; Vass 2002; Vass et al. 2005). The syn-rift stage lasted up to the Sarmatian (Serravallian) or possibly longer within the back-arc setting of the Pannonian Superbasin (Kováč 2000; Vass 2002; Vass et al. 2005). The syn-rift strata initiated with intercalations of sandstones and mudstones with fine-grained conglomerate layers deposited in shelf setting of the Karpatian age (upper Burdigalian; Fig. 2; Teriakovce Fm.; ~500 m; Vass 2002). Sedimentation of this formation is characterized by three members: (a) Lemešany conglomerates (Vass 2002), (b) Hlinné schlier (Seneš 1955; Baňacký et al. 1987), and (c) Fintice tuff (Vass 2002). The syn-rift deposition within the studied area was interrupted by salinity crises (Kotras & Džubera 1961; Karoli et al. 1997; Vass 2002; Vass et al. 2005). This event allowed sedimentation of anhydrite and halite layers intercalated with mudstones and sandstones deposited in a sabkha environment (Soľná Baňa Fm.; ~100–280 m; Vass 2002). The younger Karpatian formation is represented by multicolored, sandy mudstones (Kladzany Fm.; ~1300 m) deposited in a shallow epicontinental sea with intermittent seabed emergence (Vass & Čverčko 1985; Vass 2002). In the Prešov sub-basin, the Badenian deposits are mainly characterized by 2 formations: (1) mudstones and acidic volcanics deposited in a shelf environment (the Mirkovce Fm.; ~630 m; Kaličiak 1991; Vass 2002), (2) deltaic coarse-clastics (Klčovo Fm.; ~1700 m; Matějka 1964; Vass & Čverčko 1985; Vass 2002; Subová et al. 2022). Sarmatian sediments are only found in the southern part of the Prešov sub-basin (Fig. 2a, b) and are represented by mudstones, sandstones, rhyolitic and andesitic tuffs deposited in a deep basin setting (Stretava Fm.; ~1800 m; Vass 2002). These events were followed by basin inversion (Fig. 4; Vass 1998, 2002; Kováč 2000). For details on younger formations, refer to Vass (2002).

Data and methods

Well core samples of the Prešov-1 deep well (Ps-1) were obtained in the Gbely core repository of NAFTA Ltd. petroleum company. For the purpose of the lithological and sedimentological description of Ps-1 well core samples were cut in half perpendicular to the bedding plane and digitized. Two surface anthropogenic outcrops in the northern part of the depocenter were documented and sampled (Fig. 1). Standard sedimentological cross-section was created and lithofacies together with paleoenvironments were described according to Bouma et al. (1985), Coleman (1981), Boggs (2006), Nichols (2009), Talling et al. (2012), Patruno et al. (2015), Rossi et al. (2017) and Pellegrini et al. (2020). Basic well logs (spontaneous potential and resistivity) from the Ps-1 well were evaluated according to Emery & Myers (1996) and Rider & Kennedy (2011). Grain-size classification followed the work of Folk (1968) and Jerram (2001).

Selected thin sections were stained by epoxy blue resin for 2D total optical porosity measurement (TOP; Grove & Jerram 2011; Supplement S1). Technical details are elaborated in Suppl. S1. Total porosity and permeability (Dandekar 2013) measurements of coarse-grained rocks were performed by mercury injection method in the Unichema Ltd. Laboratory. Porosity and permeability values are evaluated based on the classification systems by Khanin (1965, 1969) and Koesoemadinata (1980). Thin section samples (Ps-1 well, Fintice and Ruská Nová Ves sections) were studied under a polarizing microscope, and selected minerals (biotite, amphibole) were further analyzed using a Cameca SX 100 microprobe (State Geological Institute of Dionýz Štúr). Minerals were verified using WDS analysis with an acceleration voltage of 15 keV, a current of 20 nA, and with a beam width of 10 μm. Raw analyzes were converted to mass percent oxides using ZAF correction.

With respect to biostratigraphy, foraminifera and calcareous nannofossils were analyzed (Ps-1 well, Ruská Nová Ves sections; Suppl. S2) to determine the age and paleoenvironment. Foraminifera has been obtained from 100 g of well core material, which was diluted by hydrogen peroxide and wet sieved (0.071 and 1 mm). The binocular stereoscopic microscope (Olympus SZ75) and the biological polarizing microscope were used for the determination of foraminifera and the scanning electron microscope QUANTA FEG 250 was used for their imaging (Institute of Electrical Engineering, SAS).

Determination of foraminifers is based on Łuczkowska (1974), Loeblich & Tappan (1992), Cicha et al. (1998), and Holbourn et al. (2013). Due to the poor preservation of the foraminiferal tests, some stay in open nomenclature. The biostratigraphic assignment is in accordance with Cicha et al. (1998) and Iaccarino et al. (2011). Calcareous nannofossils were studied from smear slides prepared by the following standard methods of sample preparation for quantitative analysis (Bown 1998). Samples were analyzed using an Olympus BX50 microscope at 1250× magnification. Camera Olympus Infinity 2, with Quick PHOTO CAMERA 2.3 software was used for the photographic record. Specimens were counted at 300 fields of view (FOV) using a quantitative method. Systematic identification of calcareous nannofossils was made by using the taxonomy of Young (1998) and Young et al. (2017). Standard nannofossil NN zonation (Martini 1971) was used for age determination.

Rhyolite conglomerate samples (amphiboles, biotites) of the Fintice (F-4, Fig. 1; Supplements S3, S4) were sent to the «Western Australian Argon Isotope Facility of Curtin University» for mineral separation and $^{40}Ar/^{39}Ar$ dating. Mineral grains were separated using Frantz's isodynamic magnetic separator and subsequently were manually selected under a binocular stereomicroscope. The sample was loaded into two 1.9 cm-diameter and 0.3 cm-depth Al discs that contain multiple smaller sample wells; all sample wells containing the separated crystals are surrounded by sample wells that carried the Fish Canyon sanidine neutron fluence monitor (28.294 [±0.13 %] Ma; Jourdan & Renne 2007; Renne et al. 2011). The sample disks were Cd-shielded (to minimize undesirable nuclear interference reactions) and irradiated for 40 h in the TRIGA reactor (Oregon State University, USA), in a central position. The correction factors for interfering isotopes were $(^{39}Ar/^{37}Ar)_{Ca}=6.95\cdot10^{-4}$ (±1.3 %), $(^{36}Ar/^{37}Ar)_{Ca}=2.65\cdot10^{-4}$ (±0.83 %) measured on CaF_2 and $(^{40}Ar/^{39}Ar)_{K}=7.02\cdot10^{-4}$ (±12 %) determined on K–Fe glass (Renne et al. 2013). Ar isotopic data are corrected for blank, mass discrimination, and radioactive decay. Individual analytical uncertainties are reported in Suppl. S3, S4 at the 1σ level unless indicated otherwise. For each sample, a series of single crystals were fused in a single step using a continuous 100 W PhotonMachine© CO2 (IR, 10.6 µm) laser fired on the aliquot material for 60 seconds. All standard crystals were fused in a single step. The gas was purified in an extra low-volume stainless steel extraction line of 240 cm^3, set up to run with two SAES AP10 and one GP50 getter. Ar isotopes were measured in static mode using a low-volume (600 cm^3) ARGUS VI mass spectrometer from the Thermo Fisher© set with a permanent resolution of ~200. Measurements were carried out in multi-collection mode using three Faraday cups equipped with three 10^{12} ohm (masses 40, 38, and 37) and one 10^{13} ohm (mass 39) resistor amplifiers and a low background compact discrete dynode (CDD) ion counter to measure mass 36. The relative abundance of each mass was measured simultaneously during 10 cycles of peak-hopping and 16 seconds of integration time for each mass. Detectors were calibrated to each other through air shot beam signals. Blanks were analyzed for every three to four incremental heating steps and typical ^{40}Ar blanks range from 1×10^{-16} to 2×10^{-16} mol. Mass discrimination was monitored using an automatic air provided a mean value of 0.991123 (±0.04 %) per Dalton (atomic mass unit). The J-value was calculated by analysing several crystals of the Fish Canyon sanidine standard and is 0.0008075 (±0.52 %). Criteria for the determination of a convergent age are as follows: (1) an age must include at least 3 consecutive single-crystals agreeing at a 95 % confidence level and satisfying a probability of fit (P) of at least 0.05. Convergent ages are given at the 2σ level and are calculated using the mean of all the individual ages, each weighted by the inverse variance of their individual analytical error. The raw data (Suppl. S3, S4) were processed using the ArArCALC software (Koppers 2002), and the ages have been calculated using the decay constants recommended by Renne et al. (2011). All analytical parameters and relative abundance values are provided in Suppl. S3, S4. Individual errors in Suppl. S3, S4 are given at the 1σ level. Convergent ages are given at 2σ include uncertainties on the decay constants and standard ages calculated using the Monte Carlo approach of Renne et al. (2010).

Description and interpretation

Ruská Nová Ves section (description)

The Ruská Nová Ves section (Fig. 1b; 48°58'51.3"N, 21°19'22.2"E) is an anthropogenic outcrop in Ruská Nová Ves village (Fig. 5a), with a height of 8.1 m comprising merged profiles P1, P3, and P4, which together create a composite section (Figs. 5b, 6). The sections generally consist of massive, occasionally laminated sandstones (Fig. 5c) and mudstones, including ripples, mud intraclasts, ?Ca concretions, soft sediment deformation, bioturbation, and fault deformations (Fig. 5d–h). The lowermost profile P1 concludes with 230 cm thick massive to laminated sandstone, while profiles P3 and P4 contain laminated mudstone and a series of sandstone layers, respectively (Figs. 5b, 6). Nine biostratigraphic samples (RNV-1 to 9) were examined, revealing a diverse range of preserved plankton tests, fossil fragments (e.g., echinoderms), and foraminifera tests. The samples also include redeposited Cretaceous plankton, shallow-water epiphytic foraminifera, and various other foraminifera species (Figs. 5b, 6; Suppl. S2). From a petrological perspective, mud intraclast samples like RNV-1 and RNV-3 are unsorted and rich in various components such as quartz clasts, glauconite, Fe-oxides, authigenic pyrite, carbonates, and clay clasts.

Ruská Nová Ves section (interpretation)

With respect to sedimentology, according to Rossi et al. (2017) sandstones in the section were likely transported by uni- and bidirectional traction, with intercalated silt, clay, and sand indicating sedimentation also via suspension, pointing to

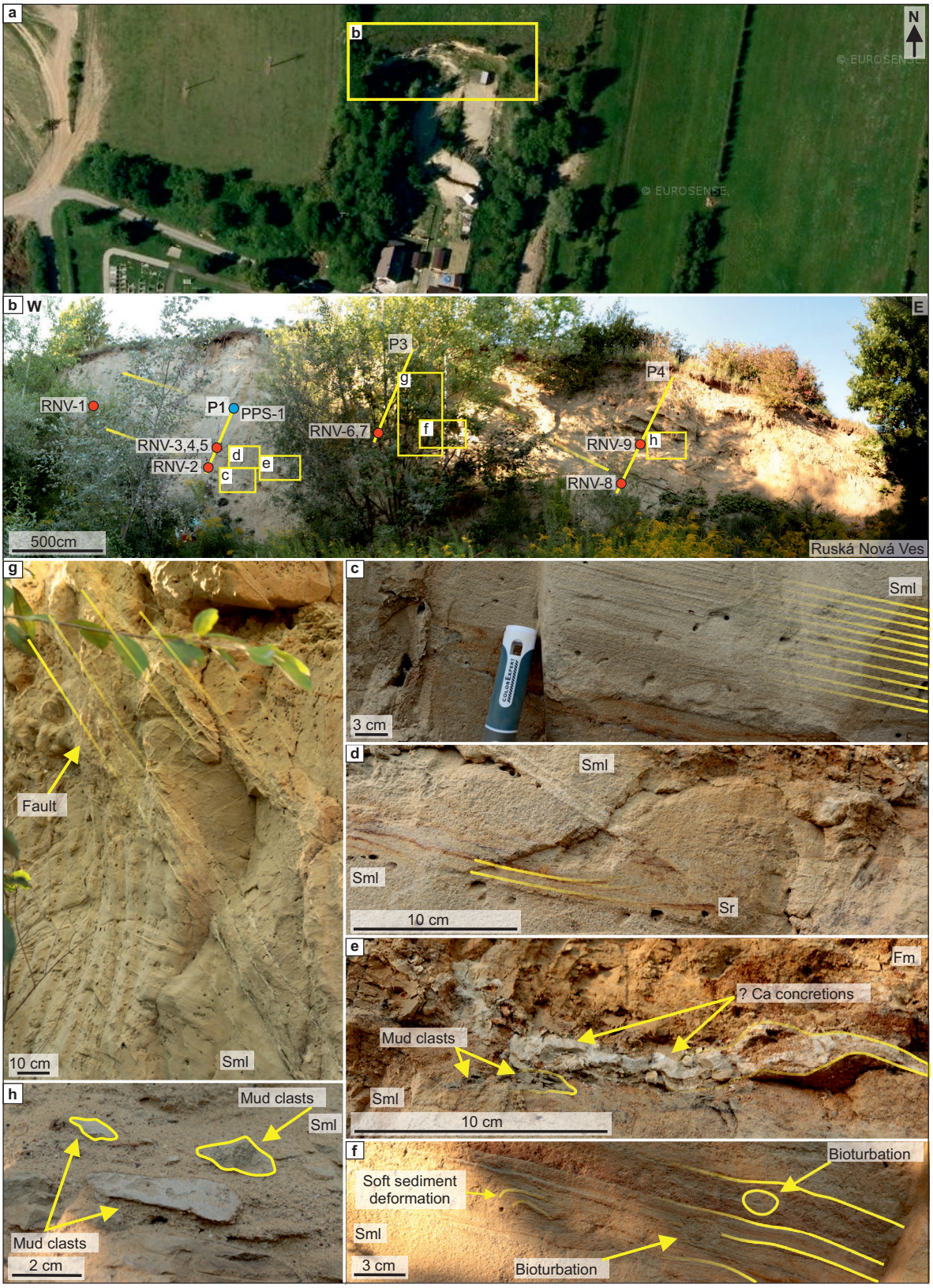

Fig. 5. The Ruská Nová Ves section (RNV). **a** — Satellite map of the location of the RNV section (mapy.cz). **b** — Detailed view of the RNV section with highlighted positions of profiles P1, P3, P4 together with petrographic (blue) and biostratigraphic (red) samples. **c** — Laminated sandstone bed. **d** — Ripple (Sr) within Sml facies. **e** — Mud intraclasts and ?Ca concretions highlighted in yellow between Sml and Fm facies. **f** — Soft sediment deformation and bioturbation within the Sml facies. **g** — Normal fault highlighted in the P3 profile. **h** — Mud intraclasts within the Sml layer highlighted in yellow. For explanations of the facies codes see Fig. 6.

a fluvial/tide-influenced environment. The presence of glauconite and echinoderm fragments suggests subaqueous marine conditions, with identified foraminifera indicating warm seawater (Fig. 6; Suppl. S2). The observed nannofossils in all samples indicate the assignment to the upper part of NN5 Zone (Figs. 5b, 6; Suppl. S2), supporting the upper Badenian age. The documented age results from mud intraclasts which are expected to be slightly older than the sandstone deposition age.

Fintice section (description)

The Fintice section (Fig. 1b; 49°02'49.2"N, 21°16'33.4"E) is situated at the southwestern end of Fintice village. The section was sedimentogically and petrologically analyzed (Figs. 7, 8a, b), but due to the barren nature of the samples, it was not possible to examine them biostratigraphically. A sedimentological profile (365 cm height; Fig. 7a–f) begins with a massive sandy-conglomerate (SGm-e), succeeded by intervals of gravelly-sandstone (GSm-e) and clast-supported conglomerate (Gmc-e; $^{40}Ar/^{39}Ar$-dated; Figs. 7, 8), all rich in rhyolite and other volcanic epiclasts. These intervals are made up of subrounded gravel and fine to coarse-grained sand. Lithofacies also contain subangular clasts of rhyolite, various minerals, and rare tuff clasts, with hematite and silicate cement (Figs. 7, 8). A sample from this section (F-4; Fig. 7a, d; Suppl. S3, S4) an epiclastic volcanic conglomerate (Gmc-e) was $^{40}Ar/^{39}Ar$-dated. The analysis of selected biotite and amphibole grains resulted in a wide age range (18 to 4 Ma), with the youngest six grains used for 11 Ma age calculation, however inverse isochron is without convergence (Fig. 8c–f). Thus, the ages are inconclusive (Suppl. S3, S4).

Fintice section (interpretation)

The Fintice section is characterized by alternating SGm-e, GSm-e, and Gmc-e facies (Fig. 7). Based on the findings of Coleman (1981), Boggs (2006) and Nichols (2009), the facies are likely formed by terrestrial debris flow deposition in an alluvial fan environment, as evidenced by the (1) lack of fossils and bioturbation, (2) red-colored GSm-e interval (from subaerial diagenetic processes), and the (3) poor to medium sorting of mineral grains and lithoclasts.

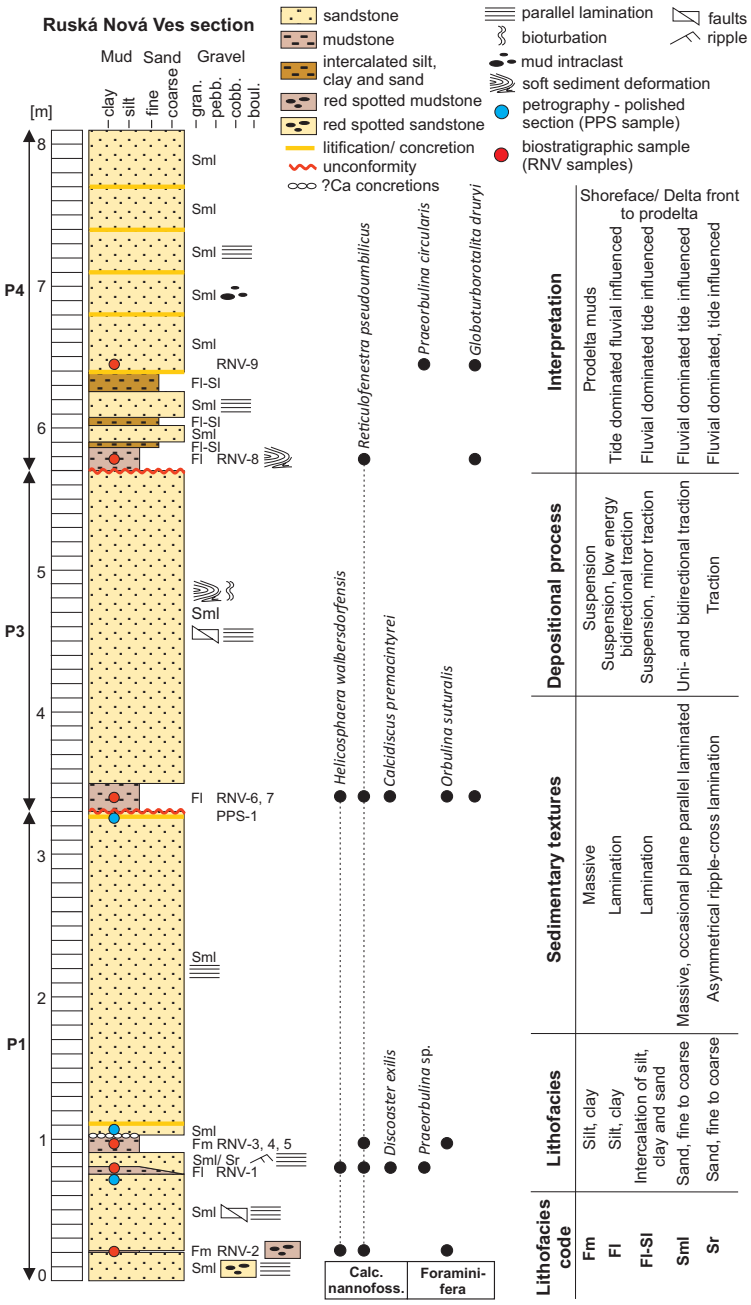

Fig. 6. Sedimentary profile of the Ruská Nová Ves section together with lithofacies codes.

Prešov-1 deep well (description)

The Prešov-1 (Ps-1; Fig. 1b; Table 1) well located in the northern part of the Prešov sub-basin (48°59'25.6753"N, 21°17'53.8425"E) includes stratotype sections for several formations (Vass 2002). The total depth of the Prešov-1 well is 3010.2 meters, including 48 well core samples (Fig. 9), 38 of which were resampled in the NAFTA Ltd. repository. Due to partially missing well core samples, data are supplemented from the original Prešov-1 well report (Čverčko 1975).

Sedimentology

The interval between 3010–2812 m (C-48 to 44; Figs. 9, 10) is composed of an alternation of gray, tectonically deformed dolomite, and sharp-edged, dolomitic breccia. Fractures

within dolomite are filled with white calcite and occasionally with pyrite. Intensive pyritization is shown at the top of this interval (C-45, 44; Čverčko 1975). In the depth of 2745–2444 m (C-43 to 37; Figs. 9, 10; Suppl. S5) dark gray, fine-grained, slightly sandy, calcareous mudstones show tectonic deformation with calcite-filled fractures. Lamination, flutes or grooves, slickensides, and carbonatized plant fragments are common (Figs. 9, 10). Dark gray breccia (C-40) contains sharp-edged clasts (~1.5 to 3 cm in diameter) composed of quartz, mudstone, dolomite, and highly micaceous metamorphic

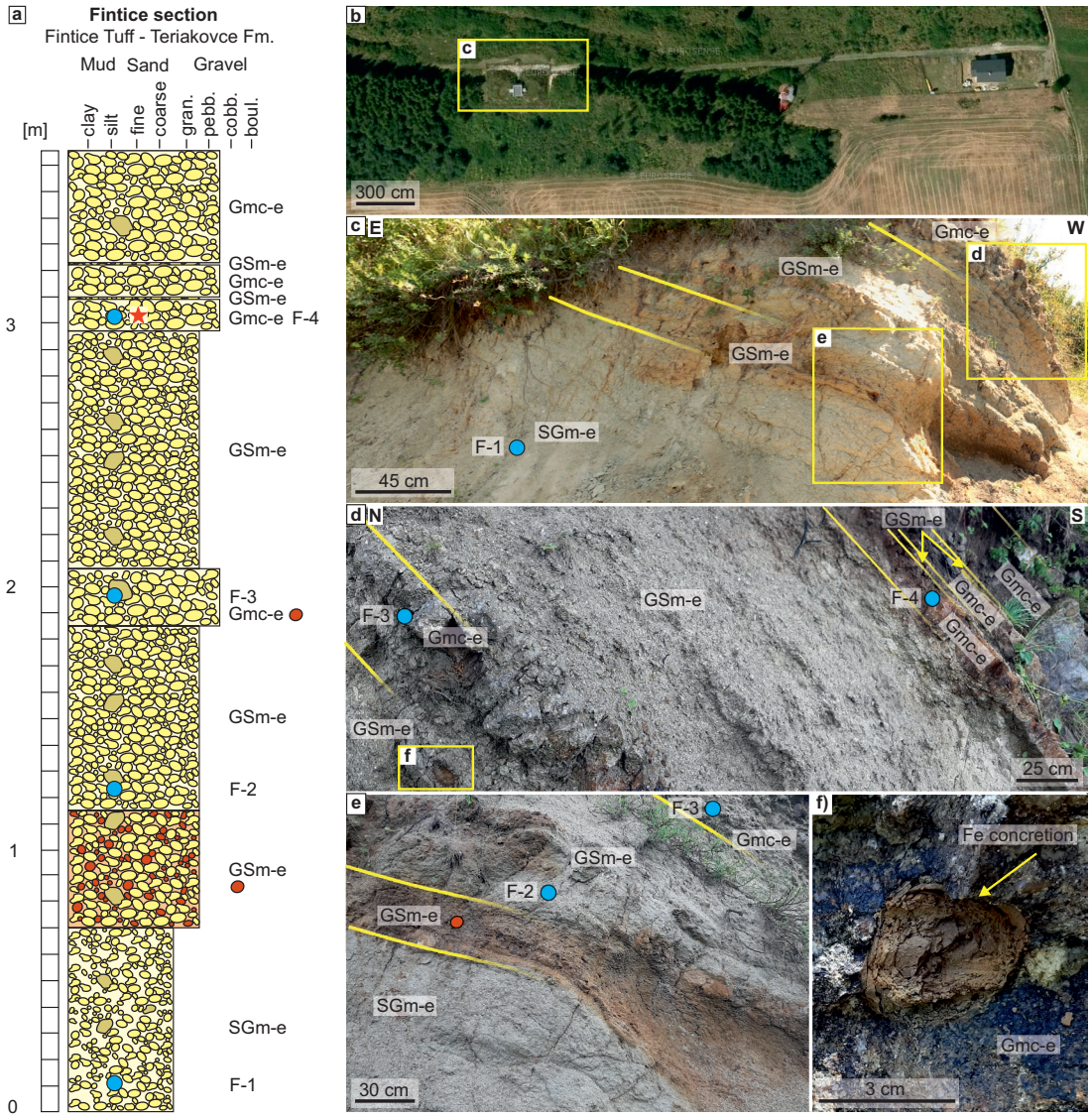

Lithofacies code	Lithofacies	Sedimentary textures	Depositional process	Interpretation
SGm-e	Sand, fine to coarse; gravel, matrix supported; volcanic epiclastic poorly sorted, subrounded clast, barren for fossils and bioturbation	Massive	Gravity transport	Terrestrial debris flow
GSm-e/ Gmc-e	Gravel, clast supported; sand, fine to coarse; volcanic epiclastic poorly sorted, subrounded clast, barren for fossils and bioturbation	Massive	Gravity transport	Terrestrial debris flow

Alluvial fan

SGm-e Sandy-conglomerate massive, volcanic epiclastic
GSm-e Gravelly-sandstone massive, volcanic epiclastic
Gmc-e Conglomerate, massive, clast supported volcanic epiclastic
Petrography - polished section (F)
$^{40}Ar/^{39}Ar$ dated sample
Fe concretion

Fig. 7. The Fintice section. **a** — Sedimentary profile of the Fintice section with lithofacies codes explanation. **b** — Satellite map of the Fintice section (mapy.cz). **c** — Detail of the Fintice section. **d** — Detailed view of the studied facies. **e** — Highlighted Fe-colored layers with Fe concretions. **f** — Fe-concretion in the Gmc-e facies.

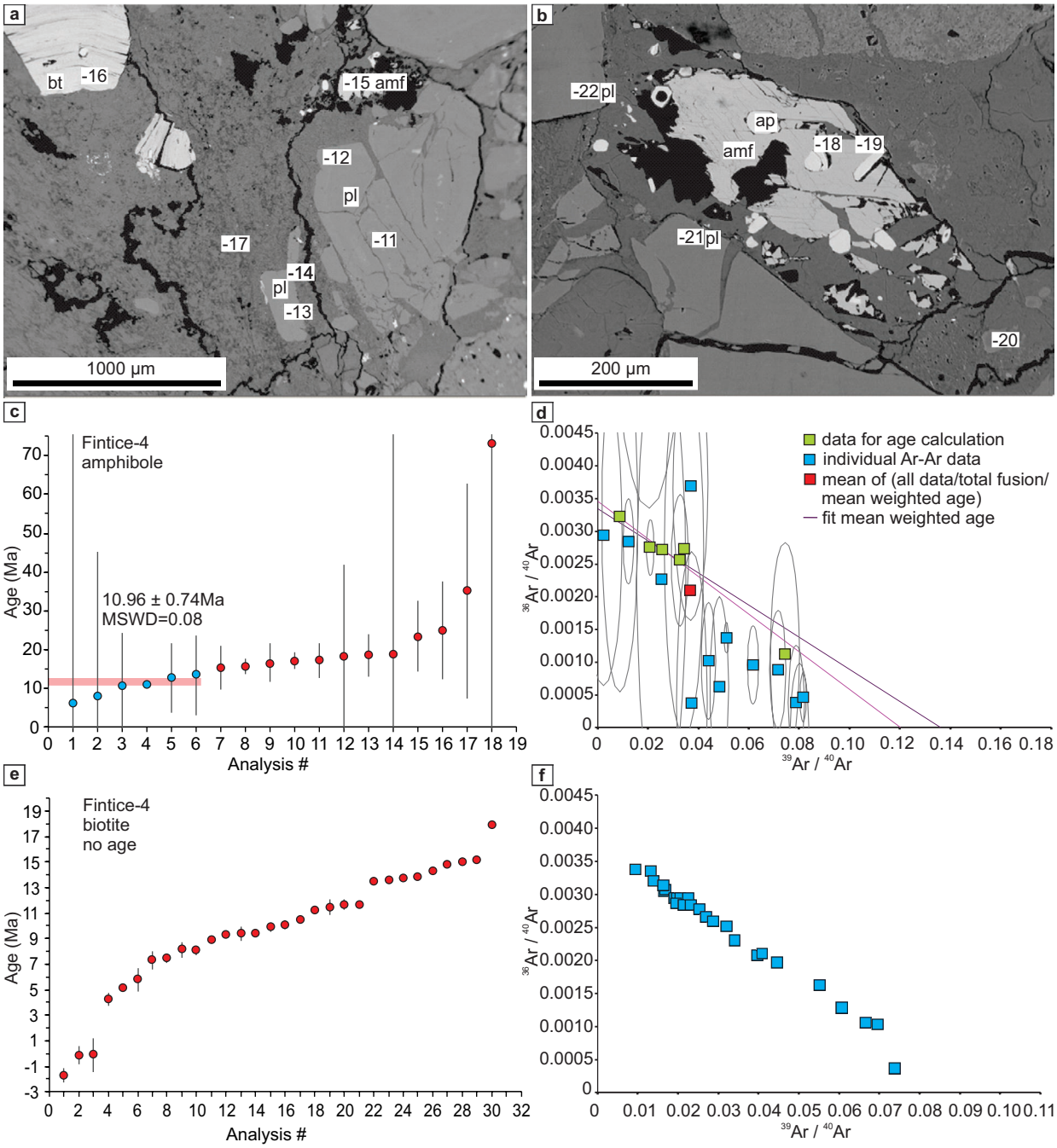

Fig. 8. Back-scattered electrons (BSE) images of rhyolite conglomerate from Fintice-4 (F-4) sample. **a** — Dated biotite together with amphibole (amf), biotite (bt) and plagioclase (pl). **b** — Dated amphibole together with plagioclase (pl) and apatite (ap). Result of $^{40}Ar/^{39}Ar$ dating. **c, d** — Amphibole converging age and inverse isochron diagrams (Fintice section); **e, f** — Biotite converging age and inverse isochron diagrams (Fintice section). See also Suppl. S3, S4.

rocks. Total porosity (Hg-porosimetry) was measured in C-37 with a value of 2.8 % and gas permeability reached a value of 0.005 mD (Tables 2, 3). Total optical porosity was measured in the same core (C-37), reaching a value of 0.27 % (Tables 2, 3). The interval between 2397–2101 m (C-36 to 30; Figs. 9, 10; Suppl. S5) is made up of dark brown to gray, massive, calcareous mudstones, and calcareous sandstones. Sediments are laminated, convolute ripple-cross and/or ripple-cross laminated, occasionally tectonically deformed. Convolute bedding, mud intraclasts, flutes or grooves and fish remains appear within this interval (Figs. 9, 10). The measured total porosity (Hg-porosimetry) reached a value of 3.4 %, the effective porosity of 0.61 % and gas permeability of 0.23 mD (C-30a; Tables 2, 3). In the depth between 2060–1147 m (C-29

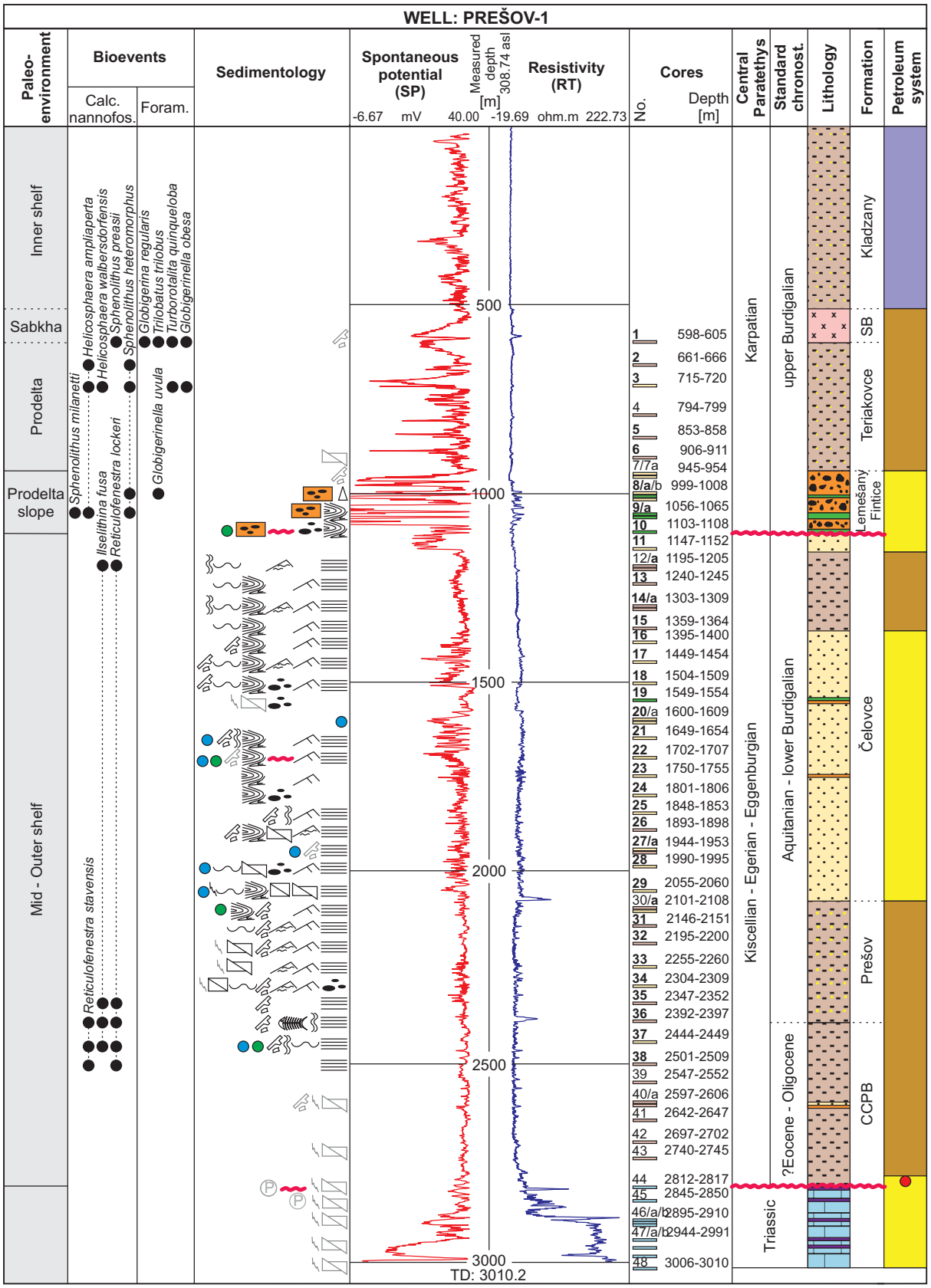

Fig. 9. Chart of the Prešov-1 well including paleoenvironment, bioevents (calcareous nannofossils and planktonic foraminifera), sedimentology, basic well logs (SP and RT extracted from Čverčko 1975), core positions with depth, age classification (international and Central Paratethys stratigraphy), lithology, formations, and petroleum system.

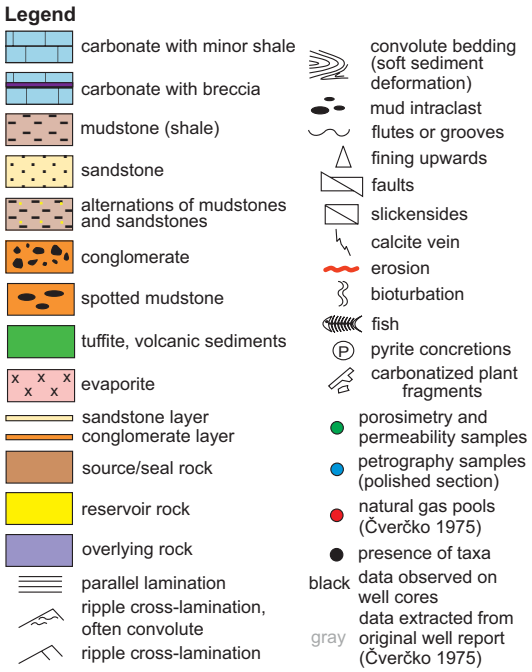

Fig. 10. Explanation for the Prešov-1 well chart.

to 11; Figs. 9, 10; Suppl. S5), sediments consist of gray to light brown sandstones, dark brown, massive mudstones, orto- and paraconglomerates. Sedimentary structures like convolute bedding (soft sediment deformation), lamination, ripple-cross, convolute ripple-cross lamination, and mud intraclasts are visible. Minor deformations, calcite fissures, bioturbation and carbonatized plant fragments appear. Flutes or grooves at the base of sandstone beds are common (Figs. 9, 10). The measured total porosity (Hg-porosimetry) reaches a value of 8.35 % and gas permeability a value of 0.36 mD (C-22; Tables 2, 3). Total optical porosity was measured in C-29, 28, 27, and 22 with an average value of 0.27 % (Tables 2, 3). The interval of 1108–945 m (C-10 to 7; Figs. 9, 10; Suppl. S5) is predominantly composed of orto- to paraconglomerates, gray to brown sandstones and brown to red spotted mudstones. Volcanic sediments occur (Čverčko 1975). Sediments are occasionally convolutely deformed. Mud intraclasts and carbonatized plant fragments are rarely developed (Figs. 9, 10). The total porosity (Hg-porosimetry) was measured with a value of 6.83 % and gas permeability of 0.01 mD (C-10; Tables 2, 3). Depth interval between 911–598 m (C-6 to 1; Figs. 9, 10; Suppl. S5) is made up of alternations of mudstones and sandstones. Tectonic deformation and carbonatized plant fragments occur (Čverčko 1975). In the depth of 598 m up to the surface, the core material is missing.

Well log facies

In the interval between 3010–2812 m (C-48 to 44; Fig. 9), the SP log shows symmetrical to bell trend with high to very high negative deflections. The RT log displays very high amplitudes with positive cylindrical, symmetrical and bell trends. For the interval 2745–2444 m (C-43 to 37; Fig. 9), a serrated trend with low excursions is typical on the SP log and a serrated trend with low amplitudes on the RT log. The interval between 2397–2102 m (C-36 to 30; Fig. 9) is represented by low to medium deflections with serrated trend on the SP log. On the RT log low amplitudes with serrated trends are present. At the base (C-36) a symmetrical trend with medium amplitude occurs. The remaining intervals are not relevant for the aims of this study and the reader is referred to Fig. 9 and Čverčko (1975).

Biostratigraphy

For biostratigraphical purposes, calcareous nannofossils and foraminifera were analyzed from rock samples (Fig. 9; Suppl. S6, S7). Among the fossils, the most abundant are very poorly preserved tests of planktonic foraminifera, porifera spines, echinoid spines, Osteichthyes bones and bivalve valves. Algae of the genus Tasmanites and Pterospermella sp. together with Diatomaceae are present. Coal, charred seeds, a lot of amorphous organic matter, and tiny foraminifera tests occur.

Prešov-1 deep well (interpretation)

Sedimentology

In the interval between 2509–1147 m (C-38 to 11), the massive sandstones were deposited from traction carpet (Ta). Laminated sandstones formed in dilute flow by low amplitude bed-waves (Tb). Ripple and/ or convolute ripple-cross laminated sandstones were deposited by dilute fully turbulent flow (Tc). Massive mudstones accumulated from gel with network of bonds (Te). According to Talling et al. (2012), such facies association most likely points to subaqueous sediment density flows. More precisely, the association can be interpreted as high density turbidites overlain by low density turbidite and

Table 2: Measured petrophysical properties from the Prešov-1 deep well.

Prešov-1 well					
Depth [m]	Core	Porosity [%]		Permeability [mD]	
		total	effective	gas	water
Data measured by the mercury injection method (Unichema Ltd.)					
1103–1108	10	6.83	–	0.01	0.001
1702–1707	22	8.35	–	0.36	0.012
2104.3–2108.3	30a	3.4	0.61	0.23	0.027
2445.5–2449.5	37	2.8	–	0.005	5.00E−05
Data determined from total optical porosity (this study)					
1702–1707	22	0.37			-
1944.5–1949.5	27	0.37			-
1990–1995	28	0.29			-
2055–2060	29	0.03			
2445.5–2449.5	37	0.27			

Table 3: Classification of petrophysical properties.

Classification of porosity and permeability (Koesoemadinata 1980)				Hydrocarbon reservoir (Khanin 1965, 1969)			
Porosity [%]	**Porosity classification**	**Permeability [mD]**	**Permeability classification**	**Class**	**Reservoir quality**	**Porosity [%]**	**Gas permeability [mD]**
0–5	very poor	<5	tight reservoir	VI	very low	<2	<1
5–10	poor	5–10	fair reservoir	VI	low	2–8	1–10
10–15	fair	10–100	good reservoir	IV	reduced	8–14	10–100
15–20	good	100–1000	very good	III	average	14–18	100–500
>25	very good		reservoir	III	high	18–20	500–1000
				I	very high	≥20	≥1000

mud. The occurrence of mud intraclasts in muddy sands (Dm-2) point to deposition by laminar or almost laminar flow, which is indicative of cohesive debris flows. Turbidites and cohesive debris flows alternate in this interval. The depositional environment can be interpreted as mid-outer shelf. In the interval between 1108–945 m (C-10 to 7), spotted muddy sands, orto- and paraconglomerates with convolute bedding, mud intraclasts (Dm-2) and gradations indicate deposition by cohesive debris flows. Red spotting suggests oxidation during exposure to the surface associated with a potential sea level fall. Depositional environment is interpreted as prodelta slope. Interval between 911–698 m (C-6 to 1) includes an alternation of massive mudstones and sandstones that were most likely deposited from suspension and low energy traction, associated with prodelta setting.

Well log facies

In the depth of 3010–2812 m (C-48 to 44), high to very high negative excursions on the SP log and very high amplitudes on the RT log indicates permeable and porous basement rocks saturated by hydrocarbons and saline water with relatively low TDS (~10,600 mg/l, Čverčko 1975). The interval between 2745–1147 m (C-43 to 11) with low to medium amplitude, predominantly serrated trend on both logs point to sandstone, muddy sands, and mudstone alternations. Negative amplitudes on the SP log seem to increase from bottom to the top. The remaining intervals are not pertinent to the objectives of this study, and readers are directed to refer to Fig. 9 and Čverčko (1975).

Biostratigraphy

Based on the analyzed samples and the evaluated association of calcareous nannofossils (Suppl. S6, S7), the interval between 2509–2347 m (Figs. 9, 10) is ranked as the NN1 to ?NN2 or older (?NP23–NP24). The reworked Oligocene nannofossils dominate, which could indicate erosion; thus the interval could also be assigned to Early Miocene Epoch. The studied assemblage in the interval of 1205–1147 m (Figs. 9, 10, Suppl. S6, S7) is ranked to the NN2 Zone with a possible transition to the NN4 Zone at the top. Thus, the depth interval between 2509–1147 m (Figs. 9, 10) is ranked to ?Kiscellian– Egerian–Eggenburian (?Oligocene to Lower Miocene). The analyzed core samples between 1062–598 m (Figs. 9, 10) with the typical association of NN4 Zone are assigned to Karpatian (Burdigalian). Due to the absence of index planktonic foraminifera (*Orbulina suturalis* or *Globoturborotalita druryi*) and presence of species with wide age range, these observations point to the fact that the studied core samples (Figs. 9, 10) should be older than Badenian. Stratigraphic outliers, which would point to Badenian age can be found in C-1 and C-3 (see Suppl. S6).

Discussion

Tectono-sedimentary development

The ?Eocene–Oligocene interval (Kiscellian to lower Egerian; Figs. 9, 10) includes subaqueous sediment density flows supported by the SP and RT logs, confirming deposition typical for a deep-water sedimentation. Biostratigraphic ranking (NP23 and NP24 zones; Suppl. S7) partly supports the Priabonian– Kiscellian age associated with the compressional foreland CCPB what is in accordance with Gross et al. (1984), Soták et al. (2001), and Starek et al. (2019). Nonetheless, no compression related structures were identified in the well data (only one well available).

The Aquitanian to lower Burdigalian deposits (Egerian to Eggenburgian; Figs. 9, 10) includes alteration of low to high density turbidite and debris flow. The RT log supports such depositional environment and biostratigraphy confirms the given age (NN2 zone; Suppl. S7). During this time, Vass (2002) describes lateral transition from the seacoast to a prograding delta. If the classification of Pellegrini (2020) is applied, the depositional environment of this interval can indeed be correlated with a mid-outer shelf, but the transition to the inner shelf was not observed by this study. The presence of glauconite and in situ bioclasts is in support of subaqueous marine environment. Based on the presence of lithoclasts, the source area most likely includes fragments from the Paleozoic basement with cover units (Veporic; Káčer et al. 2020) supported by vitrinite reflectance as well (Table 4).

Table 4: Source rock attributes from the Prešov-1 deep well (Franců 1986). For explanations see Table 5.

Franců (1986)											
Core No.	Depth [m]	Stratigraphy	Lithology	TOC [wt. %]	Rock-Eval Pyrolysis						Vitrinite Reflectance
					S1 [mg/g]	S2 [mg/g]	S3 [mg/g]	HI [mg/g]	IO	Tmax [°C]	Ro [%]
14	1305	Eggenburgian	Mudstone	0.8	0.11	0.76	0.68	95	85	427	0.55
19	1554	Eggenburgian	Mudstone	0.8	0.31	0.69	0.54	86	68	429	0.61
19	1554	Eggenburgian	Mudstone	0.8	0.06	0.66	0.44	82	54	427	0.61
27a	1951	Egerian	Mudstone	0.7	0.15	0.51	0.48	73	69	431	0.65
31	2148	Egerian	Mudstone	0.8	0.04	0.62	0.5	77	63	436	0.67
36	2397	Paleogene	Shale	0.9	0.63	0.92	0.42	108	49	435	0.63
36	2397	Paleogene	Shale	0.9	0.21	0.78	0.34	98	43	434	0.63
38	2505	Paleogene	Shale	0.7	0.06	0.56	0.47	80	67	437	0.64
42	2701	Paleogene	Shale	0.6	0.08	0.41	0.36	69	61	440	0.68
45	2848	Triassic	Shale, limestone	0.2			0.35		173		3.44
48	3008	Triassic	Dolomite	0.2			0.24		80		

This provenance is in accordance with the expected sediment entry-point from the NW to the SE (Vass et al. 2000). The ?Eocene–Oligocene to lower Burdigalian (Kiscellian to Eggenburgian) intervals represent the continuation of the older compressional foreland basin (Vass 1998, 2002; Kováč 2000). Conversely, in the other parts of the Western Carpathians the unconformity between the Paleogene and Lower Miocene sediments is evident (e.g., Biela 1978; Harzhauser et al. 2019; Vlček et al. 2020; Csibri et al. 2022). This is supported by the work of e.g. Gross et al. (1984), who documented an unconformity at the top of the Oligocene. Nevertheless, this unconformity is not observed in the Prešov depocenter. Thus, it cannot be excluded that these sediments were accumulated in one basin as e.g., in the Hungarian Paleogene Basin (Sztanó & Tari 1993; Tari et al. 1993). Above, the sedimentary record reflects gradually shallowing upwards and ends by the foreland basin disintegration and denudation during the middle Burdigalian (Ottnangian; Vass 2002).

The lower Karpatian facies (upper Burdigalian; Figs. 9, 10) dramatically change into marine to alluvial debris flows supported by the SP and RT logs. Intercalations of tuff/ tuffites were described in Čverčko (1975), which serves as an important marker bed. The presence of spotted debris flows underlines the potential exposure to the surface (oxidation) indicating a major erosional event. Biostratigraphy confirms the age classification (NN4 Zone; Suppl. S6). The tuff marker bed in the Ps-1 well seems to be lithologically connected with the surface Fintice outcrop. However, according to the results of this study, the Fintice section (this work) is barren for micro- and nannofossils what suggests lateral facies transition from the alluvial fan (Fintice section) into a prodelta slope (Ps-1 well; Fig. 9). What is generally in accordance with the interpretation of Vass (2002). The Fintice site is also linked to the 800–900 m thick ?rhyolite pyroclastics, found in the neighboring substratum of the Zlatá Baňa stratovolcano (Fig. 1b; Slávik 1968; Kaličiak 1991; Vass et al. 2000). The rare biotite paragneiss and sedimentary lithoclasts point to the redeposition of the older intervals possibly during volcano-tectonic activity. Due to disruptions in the $^{40}Ar/^{39}Ar$ radioisotope dating system, determination of the Karpatian age of the Fintice section remains unconclusive. The assignment of these rhyolitic sediments to the Karpatian age is solely based on biostratigraphy (Slávik 1968; Kaličiak 1991; Vass 2002, and this study). Continuation of the lower Karpatian interval (upper Burdigalian; Figs. 9, 10) includes prodelta facies (visible also on the SP and RT logs) ranked into the NN4 Zone as well (Suppl. S6). This sedimentary development supports the fact pointing to the foreland basin disintegration during Ottnangian and opening of the new trantensional basin within the larger back-arc basin system (Kováč 2000; Vass 2002; Fodor et al. 2021; Tari et al. 2023). Which is additionally supported by thickening of the lower Karpatian interval towards the basin controlling normal to transtensional Hornád fault system backed up by their very steep angles. Faults are defined as North–South trending and East dipping character (Grecula et al. 1977). The middle Karpatian sabkha evaporite facies follow (Fig. 9) and do not include core samples. They are only characterized by the SP log and the RT log trends (Fig. 9), which may reveal the presence of a salt formation (Emery & Myers 1996). The presence of evaporites has also been documented by Čverčko (1975) and the lithostratigraphy of Vass (2002). These salt deposits spread to the entire depocenter and were mined by the Solivar Prešov. The deposition is characterized by the precipitation of the evaporites connected with a sea-level fall which is most likely caused by geodynamic changes in the Alpine–Carpathian area (Karoli 1998; Vass 2002; Piller et al. 2007). The upper Karpatian interval (upper Burdigalian; Fig. 9) are only characterized by the SP and RT logs indicating inner shelf environment. Depositional environment is connected with a marginal marine environment with occasional surfaces of emergence (Kaličiak 1991; Vass 2002).

The Karpatian deposits are overlain by Badenian separated by unconformity (Baňacký et al. 1987; Vass et al. 2000). The Badenian (Langhian to Serravallian) sediments are situated at the eastern margin of the Prešov depocenter and younger sediments in the sub-surface (Fig. 2) are only located south of

the Drieňov–Hanušovce Horst (Řeřicha & Rudinec 1979; Vitaloš et al. 2013), which separates the Košice from the Prešov depocenter (Fig. 2). In the Prešov depocenter, the upper Badenian interval crops out in the Ruská Nová Ves section characterized by shoreface/ delta front to prodelta depositional environment (Figs. 5, 6) confirmed by this study. Thus, these sediments can be most likely linked with the Klčovo delta, which was defined by Vass (2002). It is proposed that the Klčovo delta was entering into the basin from the NW towards SE (Vass et al. 2000, 2005; Subová et al. 2022). Due to the proposed basin inversion, younger sediments are absent in the Prešov depocenter.

Petroleum system of the Prešov sub-basin

Four major source rock groups and three reservoir groups are distinguished in the Prešov sub-basin. They are described below and ordered from the stratigraphically oldest **S1** to the youngest **S4** and from **R1** to **R3** respectively. Analytical data used in this chapter have been derived from Čverčko (1975), Franců (1986), Franců et al. (1989, 1990), and this study.

The source rocks identified as S1 encompass Triassic shales along with associated Mesozoic and/or Paleozoic underlying rocks. Published data on Total Organic Carbon (TOC) from the Prešov-1 well indicate a range in quality, with TOC average values 0.2 % together with rare maximum of 1 % (Čverčko 1975; Franců 1986, Tables 4, 5). It needs to be noted that the initial values were most likely higher as indicated by very high recent maturation levels (3.44 %Ro). These formations are found beneath the entire Prešov sub-basin, as documented by e.g., Rudinec (1980) and Fusán et al.(1987), and are also exposed in nearby mountain ranges, such as the Branisko and Čierna Hora Mountains (Káčer et al. 2020). In adjacent basins, like the Vienna Basin (Rupprecht et al. 2018) and the Zala Basin (Clayton & Koncz 1994), upper Triassic deep-water shales and carbonates, including the Kössen Formation, are widely regarded as excellent source rocks. Analysis of samples from the pre-Cenozoic basement beneath the Prešov sub-basin (from the Prešov-1 well) shows an average vitrinite reflectance (%Ro) of 3.44 % (Franců 1986; Tables 4, 5). This suggests that the Triassic rocks were not thermally altered by Cenozoic burial. Additionally, these findings hint at a thermal event, likely related to upper Cretaceous nappe stacking and subsequent thermal alteration by Miocene volcanic activity. The volcanic influence is indirectly supported by the nearby Slanské Vrchy volcanic field, particularly by the basin bounding Zlatá Baňa stratovolcano (Fig. 1b; Kaličiak 1980). A similar situation is noted in e.g., the Blatné sub-basin in the Danube Basin (Rybár & Kotulová 2023), where thermal alterations are linked to buried volcanic fields.

The source rocks designated as S2 comprise mudstones from the Central Carpathian Paleogene Basin, dating to the Eocene–Oligocene epoch (Gross et al. 1984). The TOC levels suggest they are of fair quality, while the Hydrogen Index (HI) and pyrolytic S2 measurements indicate a predominance of Type III kerogen (Fig. 11a). The remaining Type IV kerogen comprises mostly inert organic matter in the form of polycyclic aromatic hydrocarbons. These have almost no potential to produce hydrocarbons (Dembicki 2017). This kerogen has reached the maturation stage necessary for oil generation (the oil window, Fig. 11b). In the Prešov sub-basin, these Paleogene formations are primarily located in the northern section and span across the entire depocenter (Fig. 2). The Central Europe, Paleogene sediments are recognized as excellent source rocks for oil production, as supported by studies such as those by Milota et al. (1995), Sachsenhofer et al. (2018), Körmös et al. (2021), Rybár & Kotulová (2023).

The source rocks identified as S3 consist of mudstones from the Egerian to Eggenburgian age, primarily associated with a Lower Miocene foreland basin, exemplified by the Prešov Formation. TOC levels suggest that these rocks are of fair quality. The Hydrogen Index (HI) and pyrolytic S2 measurements indicate the presence of Type III kerogen (Fig. 11c). Some immature samples display minor generation potential, suggesting that while the kerogen in some areas is immature, in others, it has reached the maturation phase necessary for oil generation (oil window; Fig. 11d). The Egerian to Eggenburgian mudstones are found along the entire depocenter. Generally, these sediments are classified as good oil-producing source rocks, e.g., in Alpine Foreland Basin, Carpathian Flysch Belt, Pannonian Basin (Sachsenhofer et al. 2018).

The source rocks identified as S4 consist of Badenian mudstones, primarily deposited during the transtensional rifting of the Transcarpathian Basin exemplified by formations such as the Mirkovce, Vranov, Lastomír and Klčovo (as defined by Vass 2002). TOC levels suggest that these rocks are of fair quality. The Hydrogen Index and pyrolytic S2 measurements indicate the presence of Type III and IV kerogen (Fig. 11e). Kerogen in some areas is immature, in others, it has reached the oil window (Fig. 11f). These Badenian mudstones are found exclusively in the southwest of the basin (confirmed by the Ruská Nová Ves section) and continue below the Slanské Vrchy volcanic field (Rudinec 1987, Figs. 1b, 2). Generally, these sediments are classified as good gas and wet gas producing source rocks, a categorization supported by research such as that of Franců et al. (1989, 1990).

Reservoir rocks in the Slovak part of the Transcarpathian Basin are associated with Miocene coarse-grained sandstones, volcanic sediments (Janočko 2004; Vass et al. 2005) and Mesozoic carbonates (Čverčko 1969, 1970; Rudinec 1983). Analytical data in this chapter comes from Čverčko (1975) and this study.

This work distinguishes 3 possible reservoirs in the Prešov depocenter:

- R1 (Ps-1 well; 2812–3010 m; Fig. 12) is represented by Triassic dolomites and dolomitic breccias (possibly passing into the Paleogene basal clastics). Porosity values range from 0.1 to 6.5 % (Tables 2, 3, 6), classified as very poor to poor (Koesoemadinata 1980). The permeability data from this interval remains unknown. Temperature varies between 115.5–126 °C and reservoir pressure is around

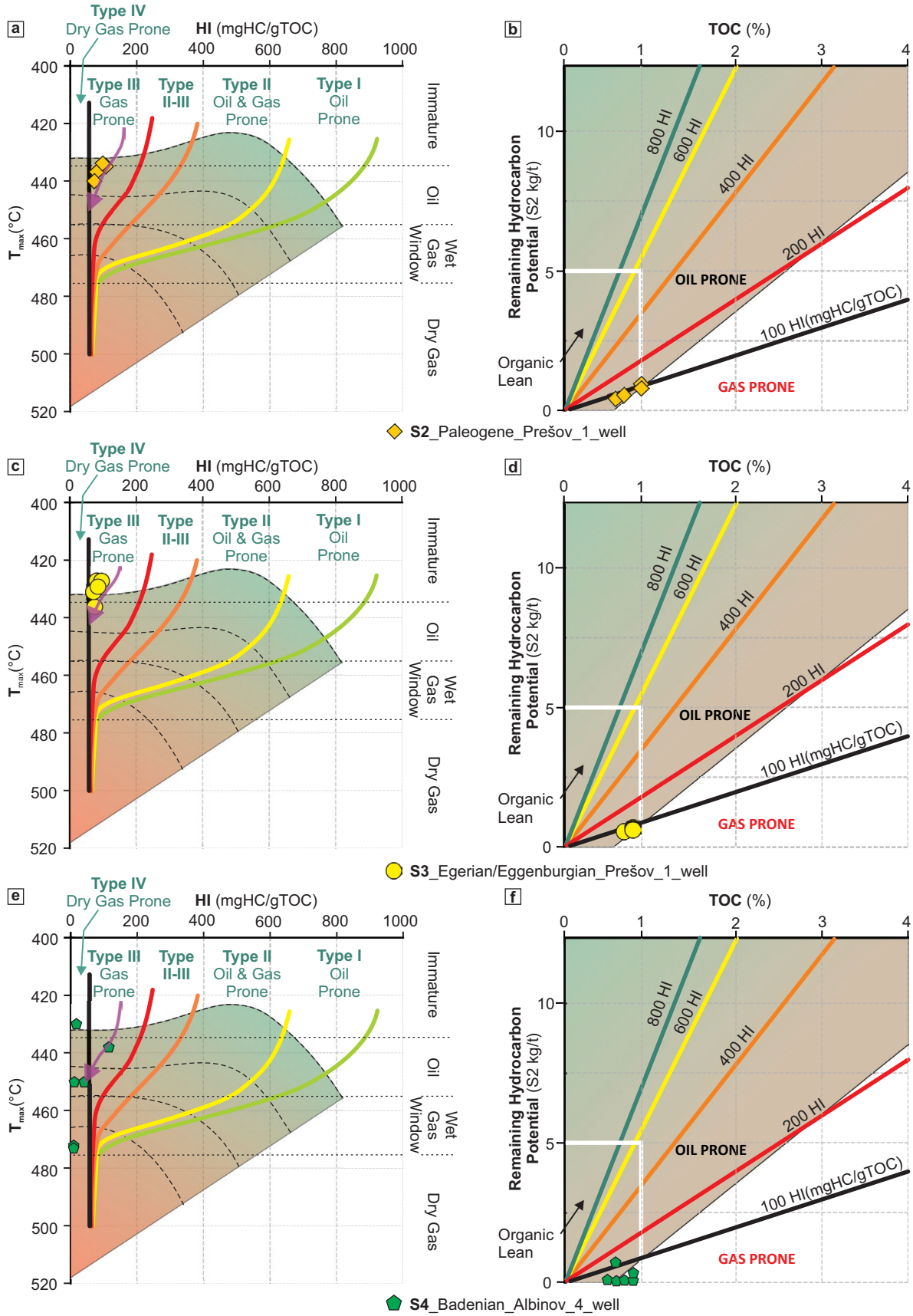

Fig. 11. a, c, e — Plot of HI versus Rock-Eval T_{max} (modified van Krevelen diagram, 1961). Purple arrow shows thermal alteration of kerogen in time. **b, d, f** — Plot of S2 versus TOC indicating the kerogen types. Data are from Franců (1986).

Table 5: Overview of the evaluated indicators of hydrocarbon potential: richness, kerogen quality, and generated hydrocarbons together with thermal maturity (Peters & Cassa 1994).

Richness			Kerogen quality and generated hydrocarbons			Thermal maturity			
Hydrocarbon potential	TOC (wt.)	Rock Eval pyrolysis – S2 (mgHC/g rock)	Rock Eval pyrolysis – HI (mgHC/gTOC)	Type	Generated HCs	Oil zones		Ro (%)	Tmax (°C); kerogen Type II/III
Poor	0–0.5	0.0–2.5	< 50	IV	Non-productive	Immature		0.2–0.6	<427
Fair	0.5–1.0	2.5–5.0	50–200	III	Gas	Mature	Early	0.6–0.65	427–435
Good	1.2–2.0	5.0–10.0	200–300	II/III	Gas+Condensate		Peak	0.65–0.9	435–442
Very Good	>2.0	>10.0	300–600	II	Oil+Condensate		Late	0.9–1.35	>442
			>600	I	Oil	Overmature		>1.35	

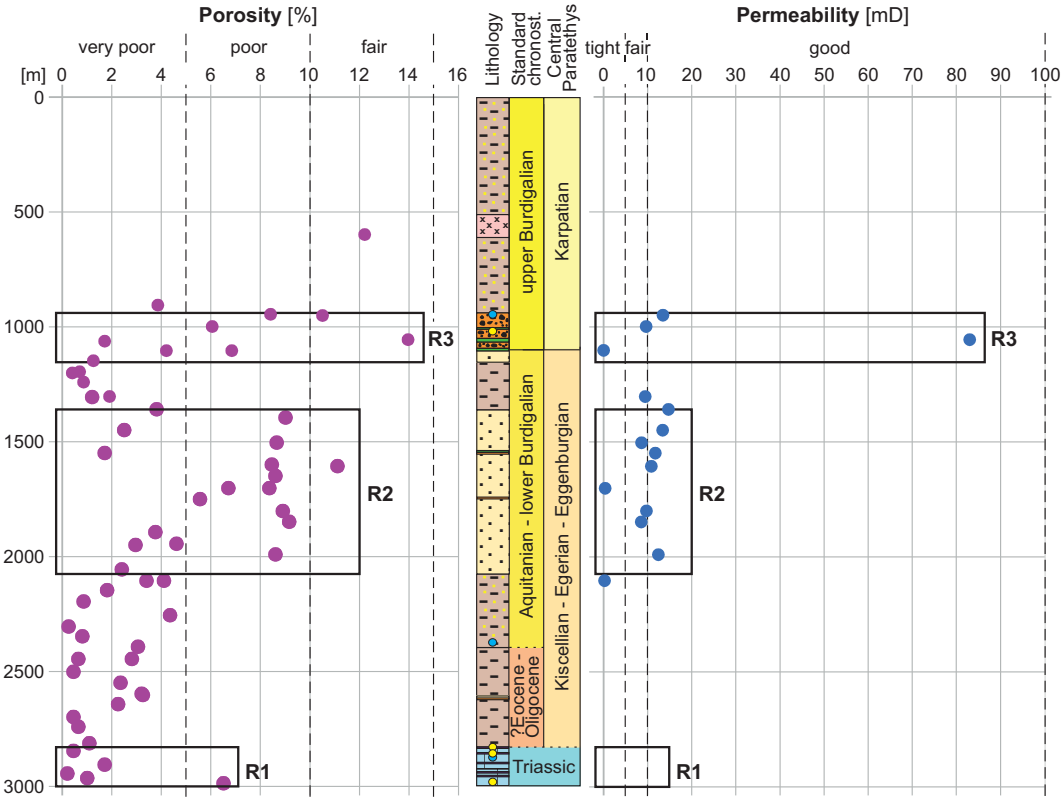

Fig. 12. Porosity and permeability vs depth, displaying reservoir bodies in the Prešov-1 well.

28 MPa (Figs. 13, 14). Reservoir water has TDS of around 10,000 mg/liter. Within this interval, three successful gas analyses have been conducted, indicating a notable presence of methane (37.3 %) and wet gas (7.3–12.4 %) at the uppermost part of the carbonate reservoir (Fig. 14; Čverčko 1975). After primary migration, the gravity separation due to molecular weight is very well documented with a predominance of CO_2 (44.01 g/mol) at the base, N_2 (28.02 g/mol) in the middle and CH_4 (16.04 g/mol) at the top (Fig. 14). Similar separation was also verified in the Danube Basin (Rybár & Kotulová 2023).

- R2 (Ps-1 well; 1147–2060 m; Fig. 12) is built by Egerian–Eggenburgian sandstones, para- and ortoconglomerates (Čelovce Fm.). Porosity reaches a value between 0.2–15.7 % (Tables 2, 3, 6), pointing to very poor to almost good quality and permeability with a value up to ~15 mD is classified as good (Koesoemadinata 1980). The quality of this reservoir is labeled as reduced (Khanin 1965, 1969). Gas analyses within this interval are not available.
- R3 (Ps-1 well; 945–1108 m; Fig. 12) is primarily composed of Karpatian para- and ortoconglomerates together with volcanic sediments (tuff, tuffites; Lemešany-Fintice Fm.). Porosity measured from rock samples reach a value between 1.4–16.8 % and permeability up to 83 mD (Tables 2, 3, 6). Based on the classification of Koesoemadinata (1980), porosity is described as very poor to good and permeability as good. Thus, the quality of reservoir is characterized as reduced (Table 3; Khanin 1965, 1969). Gas analyses

Table 6: Petrophysical and total organic carbon (TOC) values from the Prešov-1 well, extracted from the Čverčko (1975). For petrophysical and TOC classification see Tables 3, 5.

Prešov-1 well						
Depth [m]	Core	Porosity [%]		Permeability [mD]		TOC [wt%]
		Min	Max	Min	Max	
Data determined from original well report (Čverčko 1975)						
598.6–605	1	12.1	12.3			1,013
906–911	6	3.8	3.9			0.702
945–950	7	4.1	12.7			
950–954	7a	6.3	14.7	9.62	17.26	0.773
999–1004	8	2.2	9.9			0.216
1056.5–1062	9	11.1	16.8			0.114
1062–1065	9a	1.4	2			0.122
1103–1108	10	4.1	4.3			0.133
1147–1152	11	1	1.5			0.775
1195–1200	12	0.7	0.7			0.779
1200–1205	12a	0.2	0.6			0.818
1240–1245	13	0.4	1.3			0.508
1303–1306	14	1.9	-			0.776
1306–1309	14a	1.1	1.3			0.889
1359–1364	15	3.8	-			0.677
1395–1400	16	7	11			0.344
1449–1454	17	2.1	2.9	10.67	16.04	0.654
1504–1509	18	1.6	15.7			0.386
1549–1554	19	1.4	2	10.11	13.35	0.711
1600–1606	20	3.3	13.6			0.118
1606–1609	20a	10.3	11.9	9.94	11.65	0.396
1649–1654	21	6.1	11.1			1,162
1702–1707	22	0.7	12.7			0.446
1750–1755	23	1.5	9.6			0.587
1801–1806	24	3	14.8	1	18.41	0.770
1848.5–1853.5	25	7.1	11.2	8.28	8.76	1,980
1893–1898	26	3.5	4			0.970
1944.5–1949.5	27	1.2	8			0.212
1949.5–1953.5	27a	2.9	3			0.685
1990–1995	28	6.5	10.7			0.427
2055–2060	29	2.3	2.5			0.544
2104.3–2108.3	30a	2.7	5.5			0.739
2146–2151	31	1.5	2.1			0.804
2195–2200	32	0.1	1.6			0.455
2255–2260	33	3.1	5.6			1,015
2304–2309	34	0.1	0.4			1,091
2347.5–2352.5	35	0.1	1.5			0.848
2392–2397	36	1.6	4.5			0.870
2445.5–2449.5	37	0.5	0.8			0.803
2501–2505	38	0.2	0.7			0.813
2549–2552	39	2.2	2.5			1,118
2597–2602	40	2.5	3.9			0.194
2602–2607	40a	2.2	4.3			0.122
2642–2647	41	2	2.5			0.721
2697–2702	42	0.4	0.5			0.674
2740–2745	43	0.4	0.9			0.674
2812–2817	44	0.09	2.1			0.017
2845–2850	45	0.3	0.6			1,116
2905–2910	46	0.6	2.8			0.033
2944.5–2949.5	47	0.1	0.3			0.006
2964–2970	47a	0.9	1.1			0.008
2986–2991	47b	6.3	6.7			0.145
3006–3010	48					0.006

performed in this interval did not show the presence of hydrocarbon, only higher amount of N_2 (86.8 %) and CO_2 (12.2 %). Brine water with higher TDS around 76,000 mg/l is present (Fig. 14).

Prešov sub-basin play

The Prešov sub-basin (refer to Figs. 1, 2) is among the least explored and most challenging areas to access and sample within the Slovak part of Transcarpathian Basin. This is evidenced by the lack of seismic grids and the presence of only a few deep wells, among which only one is situated in the studied Prešov depocenter. The well was acquired in the 70s of the twentieth centuries and reported in detail by Čverčko (1975; Prešov-1 well).

The potential for hydrocarbon trapping within the Prešov depocenter is present due to the structural configuration of the Hornád fault system described by Grecula et al. (1977). This system is characterized by pronounced, North-South oriented normal to transtensional faults. These faults, dipping eastward towards the basin, suggest a four-way dip closure at the crest of the hanging wall block (Figs. 2, 13, 14). Additionally, the erosional unconformity observed at the Triassic sequence upper boundary, along with the presence of clastic deposits derived from the fault scarp, further define the geometry and effectiveness of this trap (Figs. 13, 14). The Triassic carbonate reservoirs, possibly extending into the basal Paleogene (identified as R1), are gas charged, including methane and wet gases (Fig. 14). The apex of these reservoirs predominantly contains methane, along with significant amounts of CO_2, N_2, and traces of H_2.

The Egerian–Eggenburgian R2 reservoirs are of limited interest due to the absence of formation waters and/or free gas. In contrast, the Karpatian conglomerate R3 does contain reservoir water and free gas; however, hydrocarbons are missing, and the reservoir predominantly contains nitrogen (see Fig. 14).

Hydrocarbons contributions from the Triassic S1 source rock into the Triassic R1 reservoir are considered unlikely due to its high thermal maturity confirmed by a vitrinite reflectance value of 3.44 % and its relatively low recent organic matter content, averaging 0.2 wt. % TOC and rarely reaching 1 wt. % TOC (Čverčko 1975; Franců 1986; Tables 4, 5, 6). However, these TOC values could have been much higher in the geological past. Similarly, charging from the Egerian–Eggenburgian S3 source rock seems improbable because of its low thermal maturity, lean TOC levels, and its stratigraphic position that does not favor migration into the Triassic R1 reservoir (Figs. 2, 14). The wet gas within the Triassic R1 trap could originate from the Badenian S4 source rock, a phenomenon commonly observed in the adjacent Trebišov sub-basin (Franců et al. 1989, 1990; Figs. 2, 14). This wet gas may have been expelled due to the thermal influence of Miocene volcanism, such as that from the neighboring Zlatá Baňa stratovolcano (Kaličiak 1980; Rudinec 1987; Figs. 1b, 2). Nevertheless, the impact of volcanoes on thermal maturity in most of the cases is local. Moreover, this hypothesis implies

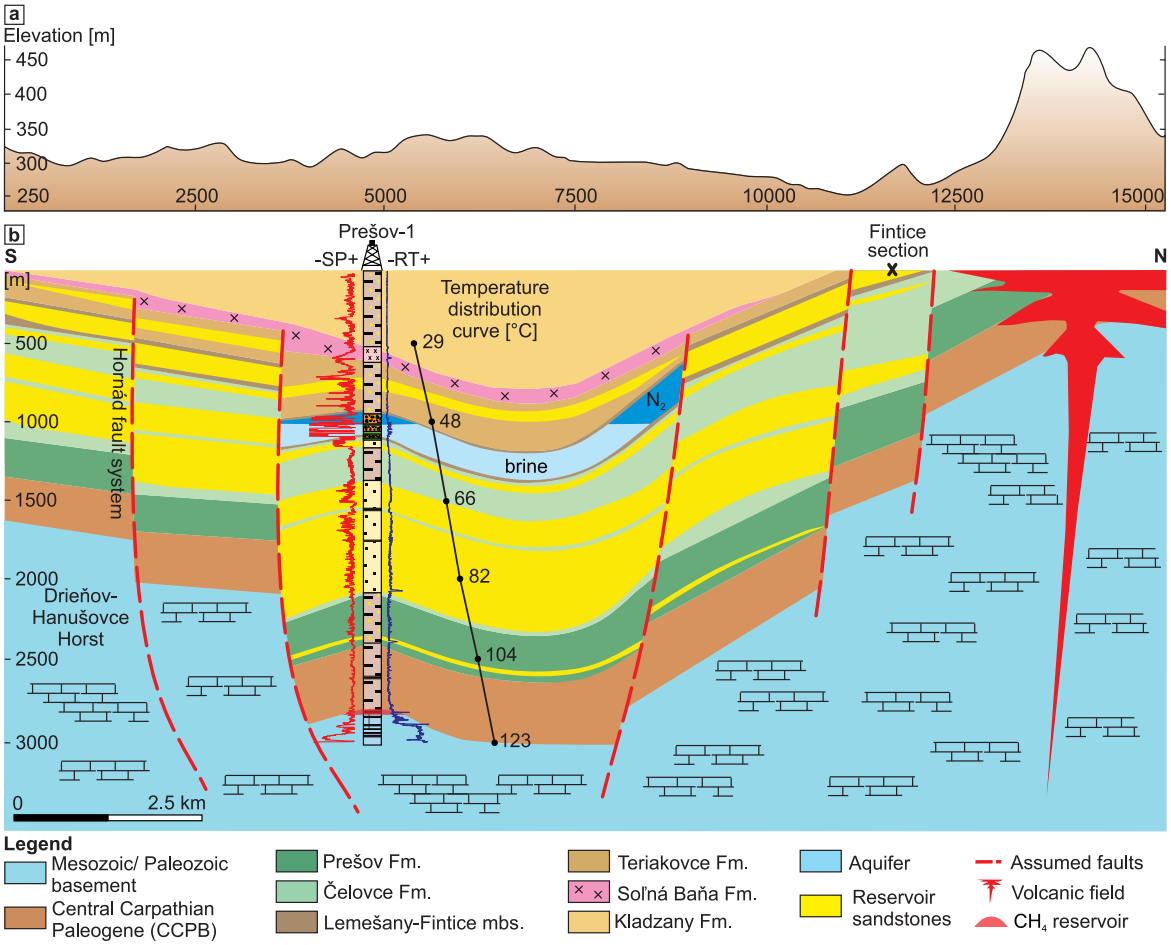

Fig. 13. a — Cross-section through the digital elevation model. **b** — Idealized south-north trending geological profile through the Prešov depocenter constructed based on available archive documents (Čverčko 1975; Filková 1976; Kaličiak 1991) highlighting temperature distribution curve. For more explanation see also Fig. 10 and for location Fig.1.

a complex and lengthy migration route, casting doubt on this scenario.

It is more likely that the R1 trap has been charged by hydrocarbons generated from the Eocene–Oligocene S2 source rocks. The early wet gases could be derived from the S2 source rocks, provided that it contains resin-derived organic matter, which has not been established yet. Future confirmation of such organic matter in S2 would suggest that early wet gases generation could occur at vitrinite reflectance values as low as 0.35 % (Tables 4, 5; Snowdon & Powel 1982; Connan & Cassou 1980). The S2 source rock is estimated to be of favorable thickness of at least ~400 meters (Čverčko 1975; this study). The Miocene rifting event placed it alongside and above the Triassic R1 reservoir, enabling both lateral and vertical hydrocarbon migration. The overlying Paleogene shales act as a seal for the Triassic R1 reservoir as well. Today, S2 falls within the early oil window (Fig. 11) and might have been producing since the Miocene, facilitated by the thick overlying Egerian–Eggenburgian and Karpatian to Badenian mudstone-sandstone overburden layers. In general, all source rocks (S1 to 4) include organic lean kerogen III type, which according to Peters & Cassa (1994) should not generate viable amounts of hydrocarbons. Despite this, the reservoir R1 contains methane gas and wet gas (Fig. 14).

A significant risk associated with CO_2 and N_2 is observed in all intervals of the R1 reservoir (Fig. 14). The CO_2 source could be linked to volcanic activity from the Zlatá Baňa structure or from the leaching of Triassic carbonate rocks. Elevated levels of CO_2 potentially stemming from volcanic processes or thermal decomposition of carbonate rocks are documented also in the NW Pannonian Basin, e.g., Répcelak and Mihályi fields, as well as in the Ivánka–Golianovo fields (Palcsu et al. 2014; Rybár & Kotulová 2023).

Geothermal potential

Analytical data used in this chapter have been derived from Čverčko (1975), Franko et al. (1995), Vranovská (2001). From the geothermal energy perspective, the carbonate R1 reservoir is located in the depth of 2812 to 3010 m (Ps-1 well; Fig. 9) and continues deeper into the basement. The lithology of this interval consists of Triassic dolomites and dolomitic breccias

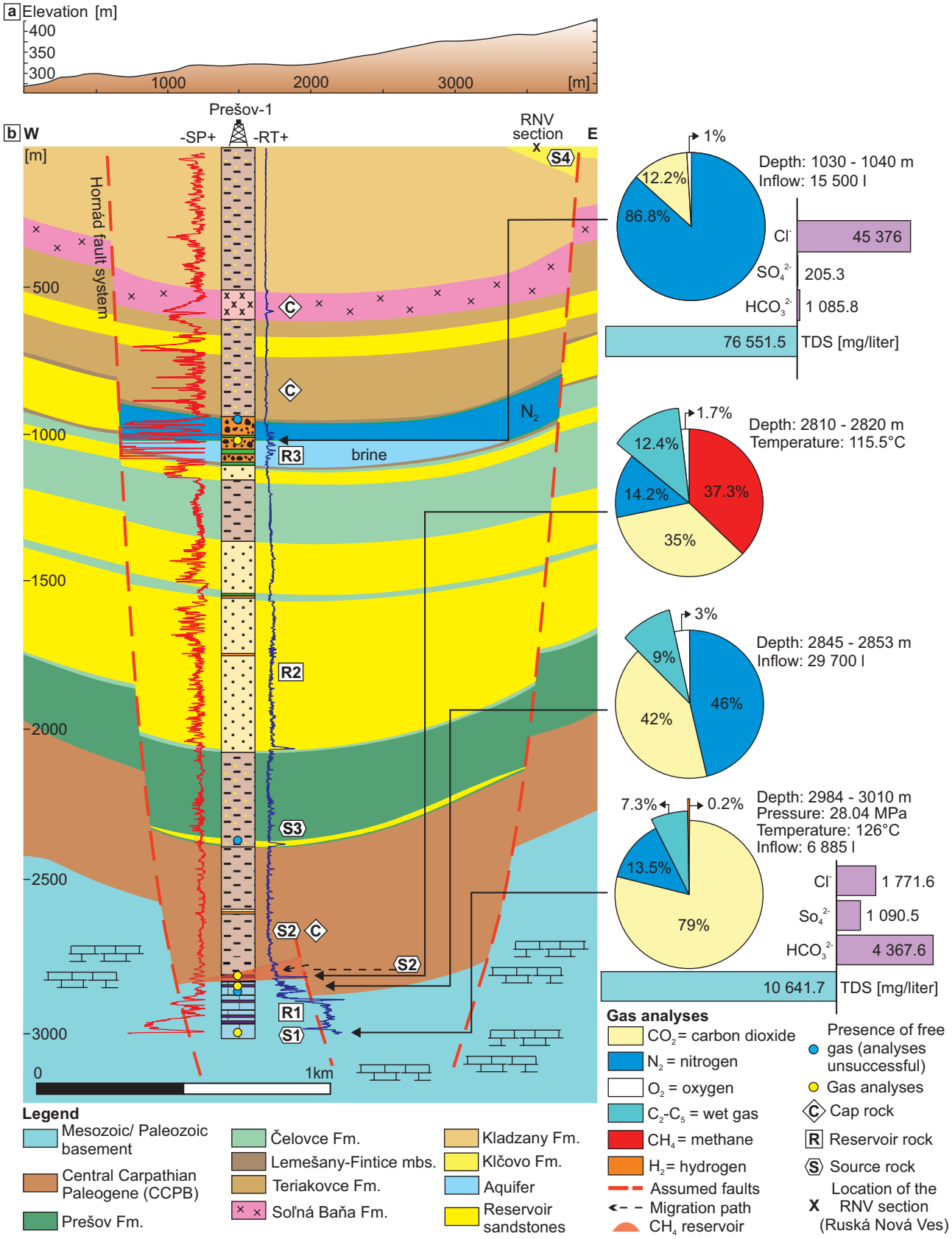

Fig. 14. a — Cross-section through the digital elevation model. **b** — Idealized West-East trending geological profile through the Prešov depocenter constructed based on available archive documents (Kaličiak 1991) highlighting gas composition and TDS analysis (Čverčko 1975). For more explanation see also Fig.10 and for location Fig.1.

with caverns. The temperature at the level of the Triassic dolomites ranges from 115.5 to 126 °C and the pressure reaches 28.04 MPa (Figs. 13, 14). The inflow from these rocks was measured to 6885 liters (2984–3010 m) to 29,700 liters (2845–2853 m; Čverčko 1975). Geothermal waters in the Prešov depocenter are described as Na-HCO_3 type with a TDS of 10 mg/l (Fig. 14; Franko et al. 1995). Compared to the Ďurkov structure (Vranovská 2001; Fig. 2), where GTD deep wells are actively used for geothermal energy, the Prešov-1 well (Figs. 13, 14) has similar properties in terms of temperature (Ps-1=126 °C; GTD=131–154 °C) and reservoir pressure (Ps-1=28.04 MPa; GTD=21.9–29.3 MPa). Benefit of the Ps-1 well is the decreased value of TDS (10,900 mg/ l), while the GTD-1, 2, 3 wells have more than 30,000 mg/l TDS (see Figs. 3, 14; Čverčko 1975; Vranovská 2001). In the Ps-1 well the TDS is still high what will cause technical difficulties due to pipeline encrustation. In conclusion, it can be said that the Prešov-1 well could meet the requirements for the use of geothermal energy. What is further exemplified by the broad study of Cloetingh et al. (2017), who also pointing out examples from the PBS and regional study by Jacko et al. (2021).

Total optical porosimetry – issues and advantages

Total optical porosimetry (TOP) measured from coarse-grained core samples of the CCPB (2444.5–2449.5 m, C=core, C-37) and the Čelovce Fm. (1990–1995 m, C-28; 1944–1953 m, C-27; 1702–1707 m, C-22) exhibit values within the range of 0.27 to 0.37 % (Tables 2, 3). These initial results of this methodology indicate significantly lower values compared to mercury porosimetry, for example in C-22 (mercury porosimetry: 8.35 %, TOP: 0.37 %; Tables 2, 3). The reasons for this deviation can be explained as follows: (a) comparison of two different methods represented by 3D (mercury porosimetry) and 2D (TOP) methods (Grove & Jerram 2011), (b) uneven distribution (polymodality) of pore space in thin sections (Carr et al. 1996), and (c) oblique cut of the analysed rock sample (Carr et al. 1996). The TOP can be improved by: (a) pore interactions with supercritical CO_2 (Berrezueta et al. 2019), (b) using several different oblique cuts together with several operators and conducting statistical analysis (Berrezueta et al. 2019), (c) experimenting with different types of epoxy resin, and (d) vacuuming the rock sample. Many authors have encountered difficulties during calibration of TOP against helium pycnometry, mercury porosimetry, nuclear magnetic resonance (NMR), CT, chemical microanalysis (Carr et al. 1996; Andreola et al. 2000; Berrezueta et al. 2019; Rubo et al. 2019).

Conclusion

In the northwest part of the Transcarpathian Basin (Prešov sub-basin), this study identified two key tectono-sedimentary events that have significantly influenced hydrocarbon potential:

- during the Eocene–Oligocene, the compressional foreland/forarc Central Carpathian Paleogene Basin was opened due to regional tectonic subsidence, which allowed source rock deposition. In the course of the Aquitanian–lower Burdigalian, the basin was disintegrated as a result of onset of back-arc extension processes of the PBS.
- the upper Burdigalian to Serravallian (or longer) rifting opened the Prešov sub-basin in a transtensional regime as a part of the larger back-arc PBS, and formed further accommodation space. This rifting resulted in the creation of faults controlling the sedimentation and deformed whole sedimentary layers, including the Triassic basement carbonates, thereby enabling the formation of hydrocarbon traps and pathways for both horizontal and vertical migration.

These significant events played a crucial role in the Prešov sub-basin petroleum play. The presented findings revalidate the potential of Paleogene sediments in Central Europe as source rocks for hydrocarbons. The specific attribute of this area is, that in contrary with the established knowledge, the organic lean kerogen type III seems to be not only producing methane gas but also wet gas. Effective hydrocarbon trap has been identified in the Triassic to basal Paleogene carbonate breccia reservoir. This reservoir presents a substantial risk of CO_2 and N_2 contamination. Interestingly, the highest concentrations of methane and wet gas were observed in the uppermost section of these carbonate traps, likely due to the gravitational separation effect, where methane, being the lightest gas, accumulates at the top. Furthermore, the geothermal potential of the Triassic dolomitic breccias explored in the Prešov-1 well appears to be moderate.

This research also examines the contrasting results obtained from total optical porosity (TOP) and mercury porosimetry. These differences are attributed to various factors, including methodological diversity and inconsistent pore distribution. To improve the accuracy and reliability of TOP measurements, the study suggests several methodological enhancements, such as optimizing interactions with supercritical CO_2, employing various angled cuts in conjunction with statistical analysis, exploring different types of epoxy resins, and applying vacuum treatment to rock samples. These improvements aim to refine our understanding of porosity and pore structure in geological samples.

Acknowledgements: This study was supported by The Ministry of Education, Science, Research and Sport of the Slovak Republic: VEGA-1/0526/21 and Excellent Grant of Comenius University Bratislava for young researchers No.: UK/3031/2024. Funded by the EU NextGenerationEU through the Recovery and Resilience Plan for Slovakia under the project No. 09I03-03-V04-00127 Special thanks go to Dr. Júlia Kotulová, Dr. M. Golej (Slovak Academy of Sciences), assoc. prof. K. Šarinová (Comenius University) and Dr. M. Šujan (EQUIS spol. s.r.o.). We express our gratitude to the editor and to the reviewers for their insightful comments, which improved the manuscript.

References

Andreola F., Romagnoli M., Leonello C. & Miselli P. 2000: Techniques used to determine porosity. *American Ceramic Society Bulletin* 79, 49–52.

Babinszki E., Piros O., Csillag G., Fodor L., Gyalog L., Kercsmár Zs., György L., Lukács R., Sebe K., Selmeczi I., Szepesi J. & Sztanó O. 2023: Magyarország Litosztratigráfiai Egységeinek Leírása II. Kainozoos Képződmények. *Szabályozott Tevékenységek Felügyeleti Hatósága*, 1–181.

Balázs A., Matenco L., Magyar I., Horváth F. & Cloetingh S. 2016: The link between tectonics and sedimentation in back-arc basins: New genetic constraints from the analysis of the Pannonian Basin. *Tectonics* 35, 6. https://doi.org/10.1002/2015TC004109

Báldi T. & Báldi-Béke M. 1985: The evolution of the Hungarian Paleogene basins. *Acta Geologica Hungarica* 28, 5–28.

Báldi-Beke M. & Báldi T. 1991: Palaeobathymetry and palaeogeography of the Bakony Eocene Basin in western Hungary. *Palaeogeography, Palaeoclimatoly, Palaeoecology* 88, 25–52.

Baňacký V., Vass D., Kaličiak M., Remšík A. & Pospíšil L. 1987: Vysvetlivky ku geologickej mape severnej časti Východoslovenskej nížiny. *The State Geological Institute of Dionýz Štúr*, Bratislava, 1–117 (in Slovak).

Berrezueta E., Domínguez-Cuesta M. J. & Rodríguez-Rey Á. 2019: Semi-automated procedure of digitalization and study of rock thin section porosity applying optical image analysis tools. *Computers & Geosciences* 124, 14–26. https://doi.org/10.1016/j.cageo.2018.12.009

Biela A. 1978: Hlboké vrty v zakrytých oblastiach vnútorných Západných Karpát. *State Geological Institute of Dionýz Štúr*, Bratislava, 1–224 (in Slovak).

Boggs S. 2006: Principles of sedimentology and stratigraphy. *Pearson Prentice Hall*, Upper Saddle River, N.J., 1–661.

Bouma A.H., Normark W.R. & Barnes N.E. 1985: Submarine Fans and Related Turbidite Systems. *Springer Verlag*, New York, 1–351. https://doi.org/10.1007/978-1-4612-5114-9_1

Bown P.R. 1998: Calcareous Nannofossil Biostratigraphy. *British Micropalaeontological Society, Publications Series*, *Chapman & Hall*, London, 1–315.

Carr M.B., Ehrlich R., Bowers M.C. & Howard J.J. 1996: Correlation of porosity types derived from NMR data and thin section image analysis in a carbonate reservoir. *Journal of Petroleum Science and Engineering* 14, 115–131. https://doi.org/10.1016/0920-4105(95)00045-3

Cicha I., Rögl F., Rupp Ch. & Čtyroká J. (Eds.) 1998: Oligocene–Miocene foraminifera of the Central Paratethys. *Abhandlungen der Senckenbergischen Naturforschenden Gesellschaft* 549, 1–325.

Clayton J.L. & Koncz I. 1994: Petroleum geochemistry of the Zala Basin, Hungary. *American Association of Petroleum Geologist Bulletin* 78, 1–22.

Cloetingh S., Van Wees J.D. & Westergom V. 2017: Thermo-mechanical controls on geothermal energy resources: case studies in the Pannonian Basin and other natural laboratories. *Acta Geodaetica et Geophysica* 52, 157–160.

Cloetingh S., Koptev A., Kovács I., Gerya T., Beniest A., Willingshofer E., Ehlers T.A., Andrić-Tomašević N., Botsyun S., Eizenhöfer P.R., François T. & Beekman F. 2021: Plume-Induced Sinking of Intracontinental Lithospheric Mantle: An Overlooked Mechanism of Subduction Initiation? *Geochemistry, Geophysics, Geosystems* 22, e2020GC009482. https://doi.org/10.1029/2020GC009482

Coe A.L. 2003: The Sedimentary Record of Sea-Level Change. *Cambridge University Press*, Cambridge, 1–287. https://doi. org/10.2277/0521831113

Coleman J.M. 1981: Deltas: Processes of deposition and models for exploration. 2nd ed., *Burgess*, 1–124.

Connan J. & Cassou A.M. 1980: Properties of gases and petroleum liquids derived from terrestrial kerogen at various maturation levels. *Geochimica et Cosmochimica Acta* 44, 1–23.

Csibri T., Ruman A., Hudáčková N., Jamrich M., Sliva Ľ., Šarinová K. & Kováč M. 2022: Deltaic systems of the northern Vienna Basin: the lower-middle Miocene conglomerate bodies. *Geologica Carpathica* 73, 245–269. https://doi.org/10.31577/GeolCarp.73.3.5

Csontos L. & Vörös A. 2004: Mesozoic plate tectonic reconstruction of the Carpathian region. *Palaeogeography, Palaeoclimatology, Palaeoecology* 210, 1–56. https://doi.org/10.1016/j.palaeo.2004.02.033

Čverčko J. 1969: Hlboký štruktúrny prieskum oblasti Ďurkov (správa za rok 1968). *Slovenské naftové závody n. p. Gbely* (in Slovak).

Čverčko J. 1970: Hlboký štruktúrny prieskum oblasti Ďurkov (správa za rok 1969). *Slovenské naftové závody n. p. Gbely* (in Slovak).

Čverčko J. 1975: Predbežná správa o výsledkoch hlbokého štruktúrneho vrtu Prešov-1. *Nafta n. p. Gbely, závod Michalovce*. (in Slovak)

Dandekar A.Y. 2013: Petroleum reservoir rock and fluid properties. Second edition, *CRC press*, UK, 1–508. https://doi.org/10.1201/b15255

Dembicki H. 2017: Practical petroleum geochemistry for exploration and production. *Elsevier*, 1–330.

Emery D. & Myers K.J. 1996: Sequences tratigraphy. *Blackwell*, Oxford, UK, 1–297. https://doi.org/10.1002/9781444313710

Filková V. 1976: Vrtno-refrakčné meranie v širšom okolí vrtu Prešov-1. *Geofond* Bratislava, číslo správy 36518 (in Slovak).

Fodor L., Balázs A., Csillag G., Dunkl I., Héja G., Jelen B., Kelemen P., Kövér Sz., Németh A., Nyíri D., Selmeczi I., Trajanova M., Vrabec M. & Vrabec M. 2021: Crustal Exhumation and Depocenter Migration from the Alpine Orogenic Margin towards the Pannonian Extensional Back-Arc Basin Controlled by Inheritance. *Global and Planetary Change* 201, 1–31. https://doi.org/10.1016/j.gloplacha.2021.103475

Folk R.L. 1968: Petrology of Sedimentary Rocks. *Hemphill Publishing Company*, Austin, 1–170.

Franců J. 1986: Katagenéza organických látok a ílových minerálov a hlavná zóna tvorby uhľovodíkov vo východoslovenskej neogénnej panve. *PhD Thesis, Geological Institute SAS*, Bratislava, 1–100.

Franců J., Rudinec R. & Šimánek V. 1989: Hydrocarbon generation zone in the East Slovakian Neogene Basin: model and geochemical evidence. *Geologica Carpathica* 40, 355–384.

Franců J., Müller P., Šucha V. & Zatkalíková V. 1990: Organic matter and clay minerals as indicators of thermal history in the Transcarpathian depression (East Slovakian Neogene Basin) and the Vienna Basin. *Geologica Carpathica* 41, 535–546.

Franko O., Remšík A., Fendek M., Fusán O. & Zvara I. 1995: Atlas geotermálnej energie Slovenska. *The State Geological Institute of Dionýz Štúr*, Bratislava, 1–164 (in Slovak).

Fusán O., Biely A., Ibrmajer J., Plančár J. & Rozložník L. 1987: Basement of the Tertiary of the Inner West Carpathians. *The State Geological Institute of Dionýz Štúr*, Bratislava, 1–123 (in Slovak).

Grecula P., Kaličiak M. & Varga I. 1977: Hornádsky zlomový systém a jeho problémy. *Mineralia slovaca* 9, 419–448 (in Slovak).

Gross P., Köhler E. & Samuel O. 1984: Nové litostratigrafické členenie vnútrokarpatského paleogénu. The State Geological Institute of Dionýz Štúr, *Geologické správy* 81, 103–117 (in Slovak).

Grove C. & Jerram D. 2011: jPOR: An ImageJ macro to quantify total optical porosity from blue-stained thin sections. *Computers & Geosciences* 37, 1850–1859. https://doi.org/10.1016/j.cageo.2011.03.002

Harangi Sz. & Lenkey L. 2007: Genesis of the Neogene to Quaternary volcanism in the Carpathian–Pannonian region: Role of subduction, extension, and mantle plume. *Geological Society of America* 418. https://doi.org/10.1130/2007.2418(04)

Hardenbol J., Thierry J., Farley M.B., Jacquin T., De Graciansky P.-C. & Vail P.R. 1998: Mesozoic and Cenozoic sequence stratigraphic framework of European basins. *SEPM (Society for Sedimentary Geology)*. ISBN 1-56576-043-3.

Harzhauser M., Theobalt D., Strauss P., Mandic O. & Piller W.E. 2019: Seismic-based lower and middle Miocene stratigraphy in the northwestern Vienna Basin (Austria). *Newsletter on Stratigraphy* 52, 221–224. https://doi.org/10.1127/nos/2018/0490

Hohenegger J., Ćorić S. & Wagreich M. 2014: Timing of the Middle Miocene Badenian Stage of the Central Paratethys. *Geologica Carpathica* 65, 55–66. https://doi.org/10.2478/geoca-2014-0004

Hók J., Šujan M. & Šipka F. 2014: Tectonic division of the Western Carpathians: an overview and a new approach. *Acta Geologica Slovaca* 6, 135–143. https://doi.org/10.1515/geoca-2016-0031

Holbourn A., Kuhnt W., Clemens S., Prell W. & Andersen N. 2013: Middle to late Miocene stepwise climate cooling: Evidence from a high-resolution deep water isotope curve spanning million years. *Paleoceanography* 28, 688–699. https://doi.org/10.1002/2013PA002538

Horváth F. 1995: Phases of compression during the evolution of the Pannonian Basin and its bearing on hydrocarbon exploration. *Marine and Petroleum Geology* 12, 837–844. https://doi.org/10.1016/0264-8172(95)98851-U

Horváth F., Bada G., Szafián P., Tari G., Ádám A. & Cloetingh S. 2006: Formation and deformation of the Pannonian Basin: constraints from observational data. *Geological Society, London, Memoirs* 32, 191–206. https://doi.org/10.1144/GSL.MEM.2006.032.01.11

Horváth F., Musitz B., Balázs A., Végh A., Uhrin A., Nádor A., Koroknai B., Pap N., Tóth T. & Wórum G. 2015: Evolution of the Pannonian basin and its geothermal resources. *Geothermics* 53, 328–352. https://doi.org/10.1016/j.geothermics.2014.07.009

Iaccarino S.M., Di Stefano A., Foresi L.M., Turco E., Baldassini N., Cascella A., Da Prato S., Ferraro L., Gennari R., Hilgen F.J., Lirer F., Maniscalco R., Mazzei R., Riforgiato F., Russo B., Sagnotti L., Salvatorini G., Speranza F. & Verducci M. 2011: High-resolution integrated stratigraphy of the upper Burdigalian–lower Langhian in the Mediterranean: the Langhian historical stratotype and new candidate for defining its GSSP. *Stratigraphy* 8, 199–215. https://doi.org/10.1515/geoca-2018-0017

Jacko S., Farkašovský R., Ďuriška I., Ščerbáková B. & Bátorová K. 2021: Critical tectonic limits for geothermal aquifer use: case study from the East Slovakian Basin Rim. *Resources* 10, 1–15. https://doi.org/10.3390/resources10040031

Janočko J. 1996: Sediment and facies of small deltas in the Eastern Slovakian Basin. *Geologické Práce* 101, 25–26.

Jerram D.A. 2001: Visual comparators for degree of grain-size sorting in two and three-dimensions. *Computers and Geosciences* 27, 485–492. https://doi.org/10.1016/S0098-3004(00)00077-7

Jourdan F. & Renne P. 2007: Age calibration of the Fish Canyon sanidine $^{40}Ar/^{39}Ar$ dating standard using primary K–Ar standards. *Geochimica et Cosmochimica Acta* 71, 387–402. https://doi.org/10.1016/j.gca.2006.09.002

Káčer Š., Antalík M., Lexa J., Zvara I., Fritzman R., Vlachovič J., Bystrická G., Brodianska M., Potfaj M., Madarás J., Nagy A., Maglay, J., Ivanička, J., Gross, P., Rakús, M., Vozárová, A., Buček St., Boorová D., Šimon L., Mello J., Polák M., Bezák V., Hók J., Teťák F., Konečný V., Kučera M., Žec B., Elečko M., Hraško I., Kováčik M. & Pristaš J. 2020: Digitálna geologická mapa Slovenskej republiky v mierke 1:50 000 a 1:500 000. *The State Geological Institute of Dionýz Štúr*, Bratislava.

Kaličiak M. 1980: Geologická stavba a vývoj neogénneho subsekventného magmatizmu v oblasti zlatobanského vulkanického aparátu (severná časť Slanských vrchov). *Mineralia slovaca* 12, 1–25.

Kaličiak M. 1991: Explanatory notes to the geological map of the northern part of Slanské vrchy Mts. and Košice depression. *The State Geological Institute of Dionýz Štúr*, Bratislava, 1–231.

Karoli S. 1998: Genéza a sedimentárne prostredie evaporitov permotriasu a neogénu. Manuscript – archive, *Geological Institute of Slovak Academy of Sciences*, Bratislava.

Karoli S., Janočko J., Kotuľák P. & Verdon P. 1997: Sedimentology of Karpatian evaporites in the East-Slovakian Neogene basin (Slovakia). *Slovak Geological Magazine* 3, 201–211.

Kázmér M., Dunkl I., Frisch W., Kuhlemann J. & Ozsvárt P. 2003: The Palaeogene forearc basin of the Eastern Alps and Western Carpathians:subduction erosion and basin evolution. *Journal of the Geological Society* 160, 413–428. https://doi.org/10.1144/0016-764902-041

Khanin A.A. 1965: Osnovnye ucheniya o porodakhkollektorakh nefti i gaza [Main Studies of Oil and Gas Reservoir Rocks]. *Publishing House Nedra*, Moscow, 1–362 (in Russian).

Khanin A.A. 1969: Porody-kollektory nefti i gaza i ikh izuchenie [Oil and Gas Reservoir Rocks and Their Study]. *Publishing House Nedra*, Moscow, 1–368 (in Russian).

Koesoemadinata R.P. 1980: Geologi Minyak dan Gas Bumi. *Institut Teknologi Bandung*, Bandung, 1–296 (in Indonesian).

Köhler E. & Salaj J. 1997: Time ranging and extend of significant Paleogene events in the Central West Carpathians. *Zemný Plyn Nafta* 41, 199–206.

Koppers A.A.P. 2002: ArArCALC – software for $^{40}Ar/^{39}Ar$ age calculations. *Computers & Geosciences* 28, 605–619. https://doi.org/10.1016/S0098-3004(01)00095-4

Körmös S., Sachsenhofer R., Bechtel A., Radovics B., Milota K. & Schubert F. 2021: Source rock potential, crude oil characteristics and oil-to-source rock correlation in a Central Paratethys subbasin, the Hungarian Palaeogene Basin (Pannonian basin). *Marine and Petroleum Geology* 127, 1–21. https://doi.org/10.1016/j.marpetgeo.2021.104955

Kotras J. & Džubera A. 1961: Záverečná správa a výpočet zásob – lokalita: Zbudza, surovina: kamenná soľ, stav k 31.12.1961. *Geologický prieskum*, Spišská Nová Ves, *Ústredný geologický úrad*, Praha, 1–335. Archive number: 11138

Kováč M. 2000: Geodynamický, paleogeografický a štruktúrny vývoj Karpatsko-Panónskeho regiónu v miocéne: Nový pohľad na neogénne panvy Slovenska. *Veda*, 1–202 (in Slovak).

Kováč M., Grigorovich A., Bajraktarević Z., Brzobohatý R., Filipescu S., Fodor L., Harzhauser M., Nagymarosy A., Oszczypko N., Pavelić D., Rögl F., Saftić B., Sliva Ľ. & Studencka B. 2007: Badenian evolution of the Central Paratethys Sea: paleogeography, climate and eustatic sea-level changes. *Geologica Carpathica* 58, 579–606.

Král M., Lizoň I. & Jančí J. 1985: Geotermický výskum Slovenska. Záverečná správa za roky 1981 až 1985. Manuskript, *Geofond*, Bratislava, 1–116 (in Slovak).

Kráľ M., Pereszlényi M. & Vass D. 1990: Vzťah rýchlosti akumulácie sedimentov ku genéze Východoslovenskej neogénnej panvy a k ložiskám uhľovodíkov. *The State Geological Institute of Dionýz Štúr*, 107–114 (in Slovak).

Lexa J., Seghedi I., Németh K., Szakács A., Konečný V., Pécskay Z., Fülöp A. & Kovacs M. 2010: Neogene-Quaternary Volcanic forms in the Carpathian–Pannonian Region: a review. *Central European Journal of Geosciences* 2, 207–270. https://doi.org/10.2478/v10085-010-0024-5

Loeblich A.R. & Tappan H. 1992: Present status of Foraminiferal Classification. In: Takayanagi Y. & Saito T. (Eds.): Studies in Benthic Foraminifera. *Tokai University Press*, 93–102.

Łuczkowska E. 1974: Miliolidae (Foraminiferida) from the Miocene of Poland Part II. Biostratigraphy, palaeoecology, and systematics. *Acta Palaeontologica Polonica* 19, 3–176. https://doi.org/10.2478/geoca-2014-0005

Lukács R., Harangi Sz., Guillong M., Bachmann O., Fodor L., Buret Y., Dunkl I., Sliwinski J., Quadt A., Peytcheva I. & Zimmerer M. 2018: Early to Mid-Miocene syn-extensional massive silicic volcanism in the Pannonian Basin (East-Central Europe): Eruption chronology, correlation potential and geodynamic implications. *Earth-Science Reviews* 179, 1–19.

Lukács R., Guillong M., Szepesi J., Szymanowski D., Portnyagin M., Józsa S., Bachmann O., Petrelli M., Müller S., Schiller D., Fodor L., Chelle-Michou C. & Harangi Sz. 2024: Mid-Miocene silicic explosive volcanism of the Tokaj Mts., eastern-central Europe: Eruption chronology, geochemical fingerprints and petrogenesis. *Gondwana Research* 130, 53–77. https://doi.org/10.1016/j.gr.2024.01.004

Martini E. 1971: Standard Tertiary and Quaternary Calcareous Nannoplankton Zonation. In: Farinacci A. (Ed.): Proceedings of the II Planktonic Conference, Roma, 1970. *Edizioni Tecnoscienza*, 739–785.

Matějka A. 1964: Vysvetlivky k prehľadnej geologickej mape ČSSR 1:200 000 M-34-XXII, Zborov – Košice. *The State Geological Institute of Dionýz Štúr*, 1–254 (in Slovak).

Milička J., Pereszlényi M. & Nagy A. 2011: Hydrocarbon potential of the Northern promontories of the Pannonian Basin System in Slovakia. *Mineralia Slovaca* 43, 351–364.

Milota K., Kovács A. & Galicz Z. 1995: Petroleum potential of the North Hungarian Oligocene sediments. *Petroleum Geoscience* 1, 81–87.

Nichols G. 2009: Sedimentology and Stratigraphy (2nd Edition). *Wiley-Blackwell*, 1–419.

Palcsu L., Vető I., Futó I., Vodila G., Papp L. & Major Z. 2014: In-reservoir mixing of mantle-derived CO_2 and metasedimentary CH_4-N_2 fluids – noble gas and stable isotope study of two multistacked fields (Pannonian Basin System, W-Hungary). *Marine and Petroleum Geology* 54, 2016–2227. https://doi.org/10.1016/j.marpetgeo.2014.03.013

Patruno S., Hampson G.J., Jackson Ch.A-L. 2015: Quantitative characterisation of deltaic and subaqueous clinoforms. *Earth-Science Reviews* 142, 79–119.

Pécskay Z., Lexa J., Szakács A., Seghedi I., Balogh K., Konečný V., Zelenka T., Kovacs M., Póka T., Fülöp A., Márton E., Panaiotu C. & Cvetkovic V. 2006: Geochronology of Neogene magmatism in the Carpathian arc and intra-Carpathian area. *Geologica Carpathica* 57, 511—530.

Pellegrini C., Patruno S., Helland-Hansen W. & Steel R.J. 2020: Clinoforms and clinothems: Fundamental elements of basin infill. *Basin research* 32, 185–205. https://doi.org/10.1111/bre.12446

Peters K.E. & Cassa M.R. 1994: Applied source-rock geochemistry. In: Magoon L.B. & Dow W.G. (Eds.): The Petroleum System. From Source to Trap. *American Association of Petroleum Geologists*, Tulsa, 93–120.

Piller W., Harzhauser M. & Mandic O. 2007: Miocene Central Paratethys stratigraphy – current status and future directions. *Stratigraphy* 4, 151–168.

Plašienka D. & Soták J. 2015: Evolution of late Cretaceous–Palaeogene Synorogenic basins in the Pieniny Klippen Belt and adjacent zones (Western Carpathians, Slovakia): Tectonic controls over a growing orogenic wedge. *Annales Societatis Geologorum Poloniae* 85, 43–76. https://doi.org/10.14241/asgp.2015.005

Ratschbacher L., Merle O., Davy P. & Cobbold P. 1991a: Lateral extrusion in the Eastern Alps, Part 1: Boundary conditions and experiments scaled for gravity. *Tectonics* 10, 245–256.

Ratschbacher L., Frisch W., Linzer H.G. & Merle O. 1991b: Lateral extrusion in the Eastern Alps, part 2: Structural analysis. *Tectonics* 10, 257–271.

Rauball J. & Tari G. 2018: Paratethyan petroleum source rocks: an overview. *Journal of Petroleum Geology* 41, 219–246.

Remšík A. 1993: Geotermálna energia Košickej kotliny. *Geologické práce* 98, 29–36 (in Slovak).

Renne P.R., Mundil R., Balco G., Min K. & Ludwig K.R. 2010: Joint determination of ^{40}K decay constants and $^{40}Ar^*/^{40}K$ for the Fish Canyon sanidine standard, and improved accuracy for $^{40}Ar/^{39}Ar$ geochronology. *Geochimica et Cosmochimica Acta* 75, 5097–5100. https://doi.org/10.1016/j.gca.2010.06.017

Renne P.R., Balco G., Ludwig K.R., Mundil R., Min K. & Min K. 2011: Response to the comment by W.H. Schwarz et al. on "Joint determination of ^{40}K decay constants and $^{40}Ar^*/^{40}K$ for the Fish Canyon sanidine standard, and improved accuracy for $^{40}Ar/^{39}Ar$ geochronology" by P.R. Renne et al. (2010). *Geochimica et Cosmochimica Acta* 74, 5349–5367. https://doi.org/10.1016/j.gca.2011.06.021

Renne P.R., Deino A.L., Hilgen F.J., Kuiper K.F., Mark D.F., Mitchell W.S., Morgan L.E., Mundil R. & Smit J. 2013: Time-scales of critical events around the Cretaceous–Paleogene boundary. *Science* 339, 684–687. https://doi.org/10.1126/science.1230492

Řeřicha M. & Rudinec R. 1979: Albinov – Vyhľadávací prieskum na živice – východoslovenský neogén. Vykonávací projekt vrtu Albinov-7. *Moravské naftové doly*, Hodonín, 33, Archive number: 43964. https://www.geology.sk/sluzby/digitalny-archiv/

Rider M. & Kennedy M. 2011: The geological interpretation of well logs (Third Edition). *Bell and Bain*, Glasgow, 1–442.

Rossi V., Perillo M., Steel R. & Olariu C. 2017: Quantifying mixed-process variability in shallow-marine depositional systems: What are sedimentary structures really telling us? *Journal of Sedimentary Research* 87, 1060–1074. https://doi.org/10.2110/jsr.2017.49

Royden L.H. & Horváth F. 1988: The Pannonian Basin: A study in basin evolution. *American Association of Petroleum Geologists*, 1–463.

Rubo R.A., Carneiro C.C., Michelon M.F. & Gioria R.S. 2019: Digital petrography: Mineralogy and porosity identification using machine learning algorithms in petrographic thin section images. *Journal of Petroleum Science and Engineering* 183, 1–14. https://doi.org/10.1016/j.petrol.2019.106382

Rudinec R. 1960: Záverečná geologická správa o pionierskom vrte Trhovište-1. *Geofond*, Bratislava (in Slovak).

Rudinec R. 1965: Záverečná geologická správa o pionierskom vrte Stretava-1. *Geofond*, Bratislava (in Slovak).

Rudinec R. 1976: Ložiská uhľovodíkov vo Východoslovenskom neogéne. *Mineralia Slovaca* 8, 289–384 (in Slovak).

Rudinec R. 1978: Paleogeographical, lithofacial and tectonic development of the Neogene in eastern Slovakia and its relation to volcanism and deep tectonics. *Geologický Zbor, Geologica Carpathica* 29, 225–240 (in Slovak).

Rudinec R. 1980: Možnosti výskytu ropy a plynu v predneogénnom podloží Východoslovenskej neogénnej panvy. *Mineralia Slovaca* 12, 507–531 (in Slovak).

Rudinec R. 1983: Správa o hlbokom vyhľadávacom vrte Kecerovské Pekľany-1. *MND k.p. Hodonín, PZ Michalovce* (in Slovak).

Rudinec R. 1987: Správa o hlbokom vyhľadávacom vrte Albínov-4. *MND k.p. Hodonín, PZ Michalovce* (in Slovak).

Rudinec R. 1989: Zdroje ropy, zemného plynu a geotermálnej energie na východnom Slovensku. *Alfa*, Bratislava, 1–162 (in Slovak).

Rupprecht B., Sachsenhofer R., Zach C., Bechtel A., Gratzer R. & Kucher F. 2018: Oil and gas in the Vienna Basin: hydrocarbon generation and alteration in a classical hydrocarbon province. *Petroleum Geoscience* 25, 3–29. https://doi.org/10.1144/petgeo2017-056

Rybár S. & Kotulová J. 2023: Petroleum play types and source rocks in the Pannonian basin, insight from the Slovak part of the Danube Basin. *Marine and Petroleum Geology* 149, 1–19. https://doi.org/10.1016/j.marpetgeo.2022.106092

Sachsenhofer R.F., Popov S.V., Coric S., Mayer J., Misch D., Morton M.T., Pupp M., Rauball J. & Tari G. 2018: Paratethyan petroleum source rocks: an overview. *Journal of Petroleum Geology* 41, 219–246.

Schmid S.M., Bernoulli D., Fügenschuh B., Matenco L., Schefer S., Schuster R., Tischler M. & Ustaszewski K. 2008: The Alpine–Carpathian–Dinaridic orogenic system: correlation and evolution of tectonic units. *Swiss Journal of Geosciences* 101, 139–183. https://doi.org/10.1007/s00015-008-1247-3

Seneš J. 1955: Výsledky geologického výskumu na území medzi Kokošovcami a Rankovcami na západnom úpätí Prešovsko-tokajského pohoria. *Geologické Práce* 4, 32–60 (in Slovak).

Slávik J. 1968: Chronology and tectonic background of the neogene volcanism in eastern Slovakia. *Geologické práce, Zprávy* 44–45, 199–214.

Snowdon L.R. & Powell T.G. 1982: Immature oil and condensate-modification of hydrocarbon generation model for terrestrial organic matter. *The American Association of Petroleum Geologists Bulletin* 66, 775–788.

Soták J. 1998: Central Carpathian Paleogene and its constraints. *Slovak Geology Magazine* 4, 203–211.

Soták J. 2010: Paleoenvironmental changes across the Eocene–Oligocene boundary: insights from the Central-Carpathian Paleogene Basin. Geologica Carpathica 61, 393–418. https://doi.org/10.2478/v10096-010-0024-1

Soták J., Biroň A., Dunkl I. & Prokešová R. 1999: Alpine Penninics in the Eastern Slovakia: From crustal updoming to basin downfaulting. *Geologica Carpathica* 50, 172–174.

Soták J., Pereszlényi M., Marschalko R., Milička J. & Starek D. 2001: Sedimentology and hydrocarbon habitat of the submarine-fan deposits of the Central Carpathian Paleogene Basin (NE Slovakia). *Marine and Petroleum Geology* 18, 87–114. https://doi.org/10.1016/S0264-8172(00)00047-7

Starek D., Soták J., Jablonský J. & Marschalko R. 2019: Turbidite sedimentology, biostratigraphy and paleoecology: A case study from the Oligocene Zuberec Fm. (Liptov Basin, Central Western Carpathians). *Geologica Carpathica* 70, 279–297. https://doi.org/10.2478/geoca-2019-0016

Subová V., Rybár S., Šarinová K., Hudáčková N., Jamrich M., Sliva Ľ., Šály B. & Hlavatý I. 2022: Evolution of the lower Badenian depositional system in the East Slovakian Basin: Implications for reservoir rock potential. *Geologica Carpathica* 73, 319–352. https://doi.org/10.31577/GeolCarp.73.4.3

Subová V., Rybár S. & Šály B. 2024: Seismic reflection data driven tectono-sedimentary analysis and hydrocarbon field characterization of the Slovak part of Transcarpathian Basin. *Geological Society of London, Collection*. https://doi.org/10.6084/m9.figshare.c.7440991.v1

Sztanó O. & Tari. G. 1993: Early Miocene basin evolution in northern Hungary: tectonics and eustasy. *Tectonophysics* 226, 485–502. https://doi.org/10.1016/0040-1951(93)90134-6

Talling P., Masson D., Sumner E. & Malgeseni G. 2012: Subaqueous sediment density flows: Depositional processes and deposit types. *Sedimentology* 59, 1937–2003. https://doi.org/10.1111/j.1365-3091.2012.01353.x

Tari G., Báldi T. & Báldi-Beke M. 1993: Paleogene retroarc flexural basin beneath the Neogene Pannonian Basin: a geodynamic model. *Tectonophysics* 226, 433–455. https://doi.org/10.1016/0040-1951(92)90345-7

Tari G., Bada G., Beidinger A., Csizmeg J., Danišik M., Gjerazi I., Grasemann B., Kováč M., Plašienka D., Šujan M. & Szafián P. 2021: The connection between the Alps and the Carpathians beneath the Pannonian Basin: Selective reactivation of Alpine nappe contacts during Miocene extension. *Global and Planetary Change* 197, 1–26. https://doi.org/10.1016/j.gloplacha.2020.103401

Tari G., Bada G., Boote D.R.D., Krézsek Cs., Koroknai B., Kovács G., Lemberkovics V., Sachsenhofer R.F. & Tóth T. 2023: The Pannonian Super Basin: A brief overview. *AAPG Bulletin* 107, 1391–1417.

van Krevelen D.W. 1961: Coal: Typology – Chemistry – Physics – Constitution. *Elsevier*, Amsterdam, 1–514.

Vass D. 1998: Geodynamic development of the Carpathian Arc in the neogene. *The State Geological Institute of Dionýz Štúr*, Bratislava, 155–188.

Vass D. 2002: Lithostratigraphy of Western Carpathians: Neogene and Buda Paleogene. *State Geological Institute of Dionýz Štúr*, Bratislava, 1–202 (in Slovak).

Vass D. & Čverčko J. 1985: Litostratigrafické jednotky neogénu Východoslovenskej nížiny. *Geologické Práce* 82, 111–126 (in Slovak).

Vass D., Elečko M., Janočko J., Karoli S., Pereszlényi M., Slávik J. & Kaličiak M. 2000: Paleogeography of the East-Slovakian Basin. *Slovak Geological Magazine* 6, 377–407.

Vass D., Pereszlényi M., Soták J. & Pipík R. 2005: Geology of the East Slovakian Basin. *Geological Institute of Slovak Academy of Sciences*, Bratislava, 1–65.

Vitaloš R., Vranovská A., Král M., Hók J., Šujan M. & Šipka F. 2013: Geologická štúdia pre projekt THERMES APVV-0724-11.

Špecializovaná geologicko–geofyzikálna analýza vo vnútorných Západných Karpatoch. *HG Service*, Bratislava

Vlček T., Šarinová K., Rybár S., Hudáčková N., Jamrich M., Halásová E., Šujan M., Franců J., Nováková P., Sliva Ľ., Kováč M. & Kováčová M. 2020: Paleoenvironmental evolution of Central Paratethys Sea and Lake Pannon during the Cenozoic. *Palaeogeography, Palaeoclimatology, Palaeoecology* 559, 1–17. https://doi.org/10.1016/j.palaeo.2020.109892

Vranovská A. 2001: Hydrogeologické a technologické poznatky z dlhodobej skúšky GTD-1, GTD-2 a GTD-3 Ďurkov. Záverečná správa, *Slovgeoterm a.s.*

Vranovská A., Král M. & Vitaloš R. 2012: Geologická štúdia pre geotermálny projekt Opiná. Čiastková správa, *HG Service*, Bratislava.

Young J.R. 1998: Neogene. In: Bown P.R. (Ed.): Calcareous Nannofossil Biostratigraphy. *British Micropalaeontological Society, Publications Series*. *Chapman & Hall*, London, 225–265.

Young J.R., Bown P.R. & Lees J.A. 2017: Nannotax3 website. *International Nannoplankton Association* (Accessed 21 Apr. 2017). http://www.mikrotax.org/Nannotax3

Electronic supplementary material is available online:

Supplement S1 at http://geologicacarpathica.com/data/files/supplements/GC-75-4-Subova_SupplS1.pdf
Supplement S2 at http://geologicacarpathica.com/data/files/supplements/GC-75-4-Subova_SupplS2.pdf
Supplement S3 at http://geologicacarpathica.com/data/files/supplements/GC-75-4-Subova_SupplS3.xlsx
Supplement S4 at http://geologicacarpathica.com/data/files/supplements/GC-75-4-Subova_SupplS4.xlsx
Supplement S5 at http://geologicacarpathica.com/data/files/supplements/GC-75-4-Subova_SupplS5.tif
Supplement S6 at http://geologicacarpathica.com/data/files/supplements/GC-75-4-Subova_SupplS6.pdf
Supplement S7 at http://geologicacarpathica.com/data/files/supplements/GC-75-4-Subova_SupplS7.pdf